~~CONFIDENTIAL~~
~~SECRET~~

Copy
RM E58C19a

NACA RM E58C19a

Copy 2

CLASSIFICATION CHANGED
To UNCLASSIFIED

NACA

By authority of NASA ltr. Date Nov. 30, 1962. By HQR

RESEARCH MEMORANDUM

dtd Nov. 14, 1962, s/Boyd C. Myers II. Effective date: June 5, 1962.

EXPLORATORY INVESTIGATION OF PERFORMANCE OF EXPERIMENTAL FUEL-RICH HYDROGEN COMBUSTION SYSTEM

By Arthur L. Smith and Jack S. Grobman

Lewis Flight Propulsion Laboratory
Cleveland, Ohio

~~CLASSIFICATION CHANGED~~
To ~~CONFIDENTIAL~~

~~By authority of NASA RM #7, Date June 2, 1958~~
~~effective date May 28, 1958~~ July 1958

I.N. 58-656
JUN 2[illegible] 1958

CLASSIFIED DOCUMENT

NATIONAL ADVISORY COMMITTEE FOR AERONAUTICS

WASHINGTON

June 25, 1958

~~SECRET~~
~~CONFIDENTIAL~~

CONFIDENTIAL

NATIONAL ADVISORY COMMITTEE FOR AERONAUTICS

RESEARCH MEMORANDUM

EXPLORATORY INVESTIGATION OF PERFORMANCE OF EXPERIMENTAL FUEL-RICH HYDROGEN COMBUSTION SYSTEM

By Arthur L. Smith and Jack S. Grobman

SUMMARY

An exploratory investigation was conducted to determine the performance characteristics of a fuel-rich hydrogen combustor; in addition, the performance of an afterburner operating with the fuel-rich exhaust mixture was evaluated. Four experimental combustors with a burning length of 18 inches were operated over a range of equivalence ratio from 7 to 26 at nominal fuel flows of 100 and 200 pounds per hour, inlet-air temperature of 80° F, and inlet pressures near 30 inches of mercury absolute. Two afterburner flameholder configurations with a burning length of 36 inches were investigated over an equivalence-ratio range from 0.2 to 1 at inlet pressures near atmospheric.

For the fuel-rich combustor, air was injected into the flowing fuel stream. In general, combustion efficiencies in excess of 90 percent were maintained over very broad ranges of equivalence ratio for all experimental combustors investigated. Some of the combustor exhaust-temperature profiles obtained were considered satisfactory in view of the preliminary nature of the test program. Combustion instability was encountered at high fuel-flow rates and high equivalence ratios with some combustors.

Two types of afterburner configuration were used. In one, the fuel-rich gas was introduced through open U-gutters normal to the airflow, and turning vanes inside the gutters were necessary to control the fuel distribution and the outlet-temperature profile. The other configuration embodied a pair of closed-end baffles perforated at the trailing edge to control the flow.

INTRODUCTION

This report describes the performance of an experimental fuel-rich hydrogen combustor (over-all hydrogen-air ratio above stoichiometric) and afterburner assembly. Various fuel-rich engine cycles using hydrogen as a working fluid as well as a fuel have been proposed for flight at high

speed and high altitude. Hydrogen's high specific heat (about 14 times as great as that of air) and its good combustion characteristics make it very desirable for these applications. In one such cycle described in reference 1, hydrogen at high pressures is heated as it passes through a heat exchanger and is then expanded through a turbine. The expanded exhaust gas is fed to a combustor where it is burned fuel-rich. This hot mixture supplies heat to the heat exchanger and then is fed to an afterburner where the remaining fuel is burned. Another similar cycle eliminates the heat exchanger by feeding the fuel-rich combustion products directly into the turbine. An analysis presented in reference 2 shows that high thrusts can be obtained by introducing additional fuel in the afterburner so that the afterburner may also be richer than stoichiometric. A fuel-rich ramjet cycle was considered in an analytical study presented in reference 3 for a propulsion system at hypersonic flight conditions.

Extensive research has been conducted on aircraft propulsion systems incorporating primary-combustor and afterburner units operating at equivalence ratios of stoichiometric and below; research on fuel-rich combustion units has been limited for the most part to analytical studies.

To evaluate the performance characteristics of a fuel-rich combustion system, preliminary tests were conducted with four fuel-rich combustors and five afterburner flameholder configurations. The primary combustors had a burning length of approximately 18 inches. These combustors, installed in a $3\frac{1}{2}$-inch-square duct, were operated at equivalence ratios from approximately 7 to 26, at pressures of about 30 inches of mercury absolute, and an inlet-air temperature of 80° F. The excess fuel was burned at equivalence ratios from 0.2 to 1 in an 8-inch circular duct simulating an afterburner.

The performance data obtained in the primary combustor and in the afterburner included combustion efficiency, outlet-temperature profile, and pressure drop.

SYMBOLS

A area, sq ft

f fuel-air ratio

f_t over-all fuel-air ratio based on total airflow, $w_{a,t}$

H chemical energy corresponding to the enthalpy values of air, combustion products, and fuel given by tables of refs. 4 and 5, 50,965.4 Btu/lb fuel

[redacted]

h	enthalpy of gas stream, Btu/lb
Δh	enthalpy rise, Btu/lb
Δh_g	measured afterburner gas enthalpy rise, Btu/lb air (based on $w_{a,t}$)
Δh_j	enthalpy rise of afterburner jacket cooling water, Btu/lb water
Δh_w	enthalpy rise of quench water, Btu/lb water
w_a	weight-flow rate of airstream, lb/sec
$w_{a,t}$	total airflow to primary combustor and afterburner, lb/sec
w_f	fuel-flow rate, lb/sec
w_w	weight-flow rate of water, lb/sec
η	combustion efficiency
ϕ	equivalence ratio, f/0.02921
Ψ_h	$h_b - h_a$, Btu/lb fuel

Subscripts:

AB	afterburner
a	air
ac	actual
b	gas b, $\left(H_2O - \frac{1}{2} O_2\right)$ as defined in ref. 4
f	fuel
j	afterburner jacket cooling water
p	primary combustor
r	reference
st	stoichiometric
th	theoretical
w	quench water

[redacted]

1 inlet station of primary combustor

2 exhaust station of primary combustor

3 afterburner inlet-air station

4 bulk temperature measuring station downstream of water quench

APPARATUS AND INSTRUMENTATION

The combustor and afterburner installation is shown in figure 1. The position of the instrumentation planes and the location of temperature- and pressure-measuring instruments in these planes are indicated. Air was supplied to the test facility from the laboratory air compressors; the hot exhaust gases from the primary combustor were fed to the afterburner where they were mixed with additional air and burned; the afterburner hot exhaust gases were cooled with air-atomized water sprays and discharged to the atmosphere. The over-all airflow was measured with a variable-area orifice located upstream of all flow-regulating valves. The airflow to the primary combustor was measured with a sharp-edged orifice plate located upstream of the primary-combustor flow-regulating valve and downstream of the main flow-regulating valves. The primary orifice was installed according to ASME specifications.

Hydrogen fuel was stored in compressed-gas cylinders. Fuel-flow rates from the cylinders to the combustor were determined from the temperature and pressure upstream of a critical-flow orifice.

The primary combustor was housed in a $3\frac{1}{2}$-inch-square duct 24 inches long. The fuel-rich exhaust was conducted through a $3\frac{1}{2}$-inch-square transition duct connected tangentially to the 8-inch-diameter afterburner. The transition duct and afterburner were water-jacketed. Inlet-air temperatures were measured at station A-A and E-E (fig. 1(a)) by bare-wire iron-constantan thermocouples. Pressures were measured at stations B-B, C-C, and D-D by static-pressure taps. The primary-combustor exhaust-gas temperature was measured at station D-D with an aspirating platinum - 13-percent-rhodium - platinum thermocouple probe supported in a water-jacketed housing. The square duct was traversed by pivoting the probe about a ball-socket connection positioned in the center of the water-cooled exhaust section. Two linear actuators mounted normal to each other (fig. 1(b)) were used to move the probe along the two axes of the square duct. The probe position was indicated by two coordinates obtained electrically from a probe position indicator. Temperatures were recorded at centers of nine equal areas as shown in figure 1(b).

Afterburner inlet pressure was measured at station E-E by a static-pressure tap. Outlet-temperature profiles at station F-F were measured with 22 platinum - 13-percent-rhodium - platinum thermocouples contained in a water-cooled support positioned as shown. The bulk gas temperature (exhaust products plus quench water) was measured at station H-H with

[redacted]

eight bare-wire Chromel-Alumel thermocouples positioned at centers of equal areas. The combustor and afterburner inlet and outlet temperatures were indicated on automatic balancing potentiometers and were not corrected for radiation or conduction. The inlet and outlet pressure data were obtained with manometers. The cooling-water flow rate for the cooling jacket and the probe was measured with a sharp-edged orifice installed according to ASME specifications. The inlet and outlet water temperatures to the water jacket were measured by iron-constantan thermocouples. The quench-water flow rate at station G-G was measured with a vane-type flowmeter. High-pressure air was used to atomize quench water for the cooling sprays. The quench water flow rate was adjusted to give complete vaporization at the bulk temperature measuring station H-H, for heat-balance determination.

Primary-Combustor Flameholders

Four fuel-rich primary-combustor designs were investigated. The design concepts employed were opposite to those normally employed for more conventional combustors. Air was injected into the flowing fuel stream. The air then burned in an atmosphere of fuel. Construction details of these combustors are shown in figure 2. The fuel-rich combustor designs consisted of flameholders mounted on both sides of an air distribution chamber (referred to herein as the air manifold, see fig. 2). In some designs air was introduced into the fuel stream through orifices located in the air manifold; in other designs the air was injected through distribution channels integral with the air manifold. The combustion length was defined as the distance from the downstream tip of the flameholder to the projected tip of the transversing probe (fig. 1(b)). The combustors were ignited by a sparkplug that was positioned to spark near the downstream face of the flameholder.

Combustor model A (fig. 2(a)) consisted of six sloping V-gutters sheltered by perforated plates. Air was directed downstream in the combustor through orifices in the end plate of the air manifold. In combustor model B (fig. 2(b)) four horizontally mounted V-gutters were connected to the air manifold by three air distribution tubes. Air in the tubes was injected into the V-gutters in an upstream direction through twelve 0.156-inch-diameter holes.

The air manifold for model C (fig. 2(c)) was connected to a cylindrical tube sealed at both ends. This manifold contained two slots 0.25 by 2.75 inches designed to direct the air upstream 50° to the burner axis. The manifold was partially enclosed by a semicircular shroud that provided a sheltered combustion zone. Fuel was admitted to the combustion zone through two 0.25- by 2.75-inch slots located in the shroud; secondary fuel entered the combustor around the shroud.

The final configuration (model D, fig. 2(d)) injected air through six slotted fins mounted on the air manifold. These slots, 0.0625 inch

wide and 0.5 inch apart, were parallel to the burner axis and decreased in length from 1.75 inch near the manifold to 0.5 inch near the tip of the fins. The slots were designed so that the air discharge would be normal to the fuel stream.

The total orifice area in the air injectors and the projected blocked area of the flameholders are indicated in the following table:

Primary-combustor model	Air-injector open area (all orifices)		Flameholder blocked area (projected)	
	sq in.	percent[1]	sq in.	percent[2]
A	0.59	37	6.36	52
B	.46	29	8.29	68
C	1.38	87	8.92	73
D	2.81	177	1.80	15

[1]Referenced to air manifold cross-sectional area, 1.59 sq in.
[2]Referenced to combustor total cross-sectional area, 12.25 sq in.

Afterburner Configurations

The fuel-rich primary exhaust gases were injected into the afterburner normal to its axis. Two basic types of afterburner flameholders, an open U-gutter and a punched-plate fuel injector (figs. 3 and 4, respectively), were used. To facilitate rapid assembly, the flameholders were installed in cylindrical sleeves as shown in the figures; a slot was cut in the cylindrical sleeve to admit the fuel. These sleeves were positioned in the afterburner with the centerline of the flameholder array intersecting the centerline of the primary-combustor exhaust transition ducting (fig. 1(b)). The afterburner was ignited by a sparkplug. For the U-gutter configurations, the afterburner reference area was 0.349 square foot.

Four modifications of the open U-gutter flameholder are shown in figure 3. Configurations 1, 2, and 3 (figs. 3(a) to (c)) consisted of an open gutter 2 inches wide and $7\frac{7}{8}$ inches long; in addition, configurations 2, 3, and 4 (figs. 3(b) to (d)) incorporated turning vanes. For configuration 4, two U-gutters, 1 inch wide and $7\frac{1}{2}$ inches long, were placed $2\frac{1}{2}$ inches between centers in the afterburner sleeve (fig. 3(d)). The projected blocked area of each of the U-gutter flameholder configurations was approximately 30 percent.

[redacted]

The punched-plate fuel injector (fig. 4) was designed by the full-scale engine group of the NACA Lewis laboratory. This design consisted of two fuel bars mounted in a 41-inch-long cylindrical sleeve. The leading edge of the bar was 0.5 inch wide and 5.81 inches long; the trailing edge, parabolic in shape, extended 11.67 inches downstream. Sixty-four fuel orifices 0.1875 inch in diameter were placed on either side of these bars, giving a total of 256 fuel orifices in all. The afterburner effective area was reduced to 0.140 square foot by inserting two plates in the cylindrical sleeve assembly. The projected blocked area of configuration 5 was approximately 29 percent. The upstream surfaces of the plates were sealed to the afterburner sleeve inlet to correspond to a 1/15 segment of a simulated full-scale engine configuration with an inner diameter of 10 inches and an outer diameter of 22 inches.

PROCEDURE

Prior to the admission of fuel, the desired primary-combustor and afterburner airflows were established at each test condition; then the primary-combustor and afterburner igniters were energized simultaneously, and the required fuel for rich operation was added. The afterburner was always operated at or below stoichiometric conditions. The inlet-air temperature was maintained at approximately 80° F. Two fuel-flow rates, 100 and 200 pounds per hour, were used. The primary-combustor equivalence ratio was varied from approximately 7 to 26; the afterburner equivalence ratio was varied from approximately 0.2 to 1. For the primary-combustor performance investigation the afterburner equivalence ratio was maintained at approximately 1. The combustor and afterburner inlet pressures varied with afterburner airflow, because no regulating valves were installed between the test facilities and the atmospheric exhaust.

COMBUSTION-EFFICIENCY CALCULATIONS

Primary Combustor

Combustion efficiency of the primary combustor was calculated by the method of reference 4 as the ratio of the actual enthalpy rise to the theoretical enthalpy rise. Since the fuel-air ratio of the primary combustor was always greater than stoichiometric, it was necessary to alter equation (15) of reference 4 to the following:

$$\eta_p = \frac{(1 + f_{st})h_{a,2} + f_{st}\psi_{h,2} + (f_p - f_{st})h_{f,2} - f_p h_{f,1} - h_{a,1}}{f_{st}H} \tag{1}$$

Values of $\psi_{h,2}$ were obtained from table I of reference 4. The enthalpy data for air and hydrogen were obtained from reference 5. The average

[redacted]

combustor exhaust temperature was obtained by averaging temperatures recorded at the centers of nine equal square areas (station D-D, fig. 1(b)).

Afterburner

The combustion efficiency of the afterburner was calculated as the ratio of the actual enthalpy rise in the afterburner to the theoretical afterburner enthalpy rise. The theoretical afterburner enthalpy rise was based on the unburned fuel leaving the primary combustor and was calculated as follows:

$$\Delta h_{AB,th} = f_t H - \eta_p f_{st} H \frac{w_{a,p}}{w_{a,t}} \tag{2}$$

The use of equation (2) implies that there was no additional burning between station 2 and the afterburner fuel inlet. The maximum error that could occur from this assumption for the data herein would be a 3-percent reduction in afterburner efficiency.

The actual enthalpy rise for the afterburner was calculated from a heat balance based upon afterburner gas enthalpy rise, heat rejection to the water jacket, and heat absorption by the water-quench spray according to the relation

$$\Delta h_{AB,ac} = \Delta h_g + \Delta h_w \frac{w_w}{w_{a,t}} + \Delta h_j \frac{w_{w,j}}{w_{a,t}} \tag{3}$$

The afterburner gas enthalpy rise Δh_g was calculated as follows:

$$\Delta h_g = (1+f_t)h_{a,4} + f_t \psi h_{,4} - h_{a,3} \frac{w_{a,AB}}{w_{a,t}} - \frac{w_{a,p}}{w_{a,t}} \left[(1+f_{st})h_{a,2} + f_{st}\psi h_{,2} + (f_p - f_{st})h_{f,2} \right] \tag{4}$$

The enthalpy data for water were obtained from reference 6.

RESULTS AND DISCUSSION

This report presents performance data obtained with combustors operating at over-all fuel-air ratios greater than stoichiometric, and performance data obtained with afterburners that burned the combustor fuel-rich exhaust products. Calculated data presented in figure 5 make it possible to compare performance data obtained with the fuel-rich combustor

with more conventional combustors on the basis of the inlet mass flow per combustor frontal area. The primary-combustor exhaust Mach number is related to equivalence ratio for two values of fuel flow and several values of airflow per combustor frontal area (12.25 sq in.) in the figure. The experimental data for the primary combustor and afterburner obtained during the investigation are presented in tables I and II, respectively.

Performance of Fuel-Rich Combustor

Combustion efficiency. - The combustion efficiencies obtained over a range of primary-combustor equivalence ratios with the four primary-combustor models are presented in figure 6. Data presented for model A were obtained at pressures of 30 to 51.5 inches of mercury absolute. Data for models B, C, and D were obtained at constant inlet pressure at about 30 inches of mercury absolute and with the afterburner operating at an equivalence ratio near 1.

CK-2

Combustion-efficiency data obtained with model A for three inlet fuel flows, various inlet pressures, and a range of equivalence ratios are shown in figure 6(a). The figure shows a spread in combustion efficiency of about 35 percent over most of the equivalence-ratio range. This scatter cannot be traced to the pressure variation but seems to be due to combustion instability. This instability may be attributed to the lack of formation of the proper local fuel-air mixture distribution in regions behind the flameholder. Since the air was injected axially in the combustor, fuel-air ratios in the wake of the flameholders may have exceeded the maximum flammability limit for hydrogen. Stable and efficient combustor operation requires a design providing considerable heat release in the recirculatory region. In the fuel-rich combustor, the air is liable to be deficient; consequently, variations in efficiency and stability might be associated with the manner of air introduction.

The combustion efficiency of model B is shown in figure 6(b). In general, combustion efficiencies in excess of 90 percent were maintained up to equivalence ratios near 16; above this value decreases in combustion efficiency and ultimately flame blowout were encountered.

The design principles employed with hydrocarbon fuels for jet-engine combustors were utilized in the design of model C. A shroud was installed around the air manifold in an attempt to control the rate at which fuel was mixed with the air and to provide approximately stoichiometric fuel-air ratios in this sheltered region. Fuel was admitted through slots in the shroud, and the air was injected in an upstream direction to intercept and mix with the incoming fuel. The remaining fuel flowed around the shroud and diluted the hot exhaust gases. Results obtained with model C are shown in figure 6(c). At the low inlet fuel flow, stable operation with combustion efficiencies near 100 percent was maintained over the

equivalence-ratio range tested. At the high inlet fuel flow, combustor blowout was encountered at an equivalence ratio near 18. The performance data obtained with this combustor indicate that more favorable conditions for combustion were obtained than with models A and B; however, the blowout encountered at the high inlet fuel flow suggests that further improvement in mixture distribution is required.

The model D combustor was designed so that sheets of air would be injected normal to the fuel stream. The performance data obtained with this combustor are presented in figure 6(d). Stable operation was maintained with this model over the entire operating range considered. Equivalence ratios as high as 25 were investigated at both fuel-flow conditions, and no flame blowout was observed. Combustion efficiencies near 100 percent were maintained at the low fuel flow; at the higher fuel flow, however, combustion efficiencies decreased to values near 90 percent. The stability exhibited by model D may be attributed to the increased number of air-injection stations and to the air-injection direction, which resulted in a more even distribution of the air.

Air-injector pressure loss. - The air-injector pressure losses obtained with the four primary-combustor models are presented in figure 7 as the ratio of the total-pressure loss across the air-injector to the inlet total pressure. The highest pressure losses (35 to 55 percent) were obtained with model B at the high fuel-flow condition. The pressure losses obtained with the four combustors follow the trends that might be expected from the varying open-hole areas. In this investigation no attempt was made to refine the combustor designs; it seems probable that considerable reduction in air-injector pressure loss could be effected, especially in model B.

Combustor static-pressure loss. - The static-pressure loss across the combustor is shown for four-primary combustor models in figure 8. This figure shows the variation of the ratio of static-pressure loss across the combustor to combustor inlet static pressure with equivalence ratio for fuel flows of 100 and 200 pounds per hour. The inlet static pressure measured at the plane of the flameholder was corrected for the flameholder area blockage to the static pressure at the combustor reference area. Static-pressure loss for all configurations was less than 5 percent.

Combustor outlet-temperature profiles. - The representative outlet-temperature profiles (18 in. from flameholder) of the four primary-combustor models are shown in figure 9. The circles on the figures indicate probe positions. The recorded temperature values appear near these circles. The isotherms on the figures were approximated. In general, the temperature patterns obtained at other test conditions were similar to those presented in the figure. In figures 9(a) and (b) temperature profiles are presented for model A operating at combustion efficiencies of approximately 72 and 100 percent, respectively. The difference between

the maximum and minimum values in figure 9(a) was 1295° F; this difference was 700° F for data presented in figure 9(b). These variations in profile and efficiency seem to imply that partial blowout was obtained with model A, since these data were obtained at approximately the same operating conditions.

The temperature pattern at the outlet of model B (fig. 9(c)) represents a large improvement over that obtained with model A. The difference between maximum and minimum temperatures is only 245° F. Model C (fig. 9(d)) produced an outlet profile better than that obtained with model A but not as good as that obtained with model B. The difference between maximum and minimum temperatures for model C is about 415° F. Model D (fig. 9(e)) produced a nonuniform temperature profile. The difference between maximum and minimum temperatures is about 915° F. No design changes were made to flatten these profiles.

Afterburner Performance

The effect of various afterburner flameholder designs on afterburner performance was observed over a range of afterburner equivalence ratios for fuel flows of 100 and 200 pounds per hour and afterburner inlet-air temperatures of 80° F. Afterburner airflow was varied to obtain a variation in afterburner equivalence ratio. The pressure in the afterburner increased with increasing afterburner airflow (reductions in afterburner equivalence ratio). Primary-combustor model A operating at equivalence ratios of approximately 10 and 20 supplied the fuel-rich exhaust mixture for the afterburner performance tests.

The calculated variation of afterburner reference Mach number with afterburner equivalence ratio is shown in figure 10. The reference Mach number is based on the total cross-sectional area of configurations 4 and 5. Increasing equivalence ratio (by decreasing airflow) reduces the Mach number.

Afterburner temperature profile. - The effect of flameholder design on temperature profile is shown in figure 11. Representative curves are presented for the five flameholder configurations. The flameholders were positioned as shown in figure 1(b). The effective airflow and fuel-flow areas were the same for all four U-gutter configurations. This area was different for the punched-plate fuel ejector; consequently, the two designs cannot be compared directly.

The simple U-gutter (config. 1, fig. 3(a)) gave an outlet-temperature pattern very hot on bottom and cold on top (fig. 11(a)). Apparently the momentum of the incoming fuel-rich gas caused it to flow down the gutter, mix, and burn on the bottom of the duct. In an attempt to distribute the fuel more uniformly in the afterburner, a series of U-gutters with

turning vanes was investigated. Configuration 2 (fig. 3(b)) incorporated three turning vanes; the results obtained are shown in figure 11(b). The temperature profile obtained with this configuration was similar to that observed with configuration 1, but a slight improvement in the profile was indicated. A portion of the lower thermocouple rake failed because of high temperature along the bottom of the duct.

Three vanes extending $9\frac{1}{2}$ inches in an axial direction from the fuel inlet slot were employed in configuration 3 (fig. 3(c)). The results obtained are shown in figure 11(c). The temperature pattern was better than that obtained with configuration 1 or 2. The pattern along the bottom is much flatter than that at the top, and the average temperature is higher. The need for improving the lateral distribution of the fuel in addition to the radial distribution is evident. To obtain lateral distribution of the fuel as well as radial distribution, a double U-gutter (config. 4, (fig. 3(d)) employing seven turning vanes with some of the vanes turned toward the top of the afterburner on the discharge side was investigated. The results obtained with this configuration are shown in figure 11(d). The over-all temperature profile was greatly improved with this configuration.

The afterburner was modified for tests with configuration 5 (fig. 4) to simulate the area ratios encountered in a simulated full-scale test setup. A 1/15 segment of a full-scale afterburner was installed within a cylindrical sleeve and inserted into the afterburner for these tests. The representative temperature profile obtained with this configuration is shown in figure 11(e). There is a tendency for the top of the afterburner to be somewhat hotter than the bottom; considering the area change between the top and bottom, however, this profile is considered good.

Afterburner combustion efficiency. - The combustion efficiencies of the two flameholder configurations that gave the best profiles (configs. 4 and 5) are shown in figure 12 as a function of the over-all equivalence ratio. Since the test facility discharged to atmospheric pressure, the afterburner inlet pressure varied with operating conditions. This pressure variation was from 30 to 38 inches of mercury with configuration 4 and from 31 to 55 inches of mercury with configuration 5. The data in figure 12 are presented for two primary-combustor equivalence ratios and for two fuel flows. In general, combustion efficiencies in excess of 90 percent were observed for configurations 4 and 5 over the range of afterburner equivalence ratio considered. The performance of the two configurations is not directly comparable because of the differing inlet velocities (fig. 10).

Fuel-rich gas-injector pressure loss. - Figure 13 presents the pressure losses associated with the injection of the hot fuel-rich gases from the primary combustor into the afterburner for models 4 and 5. This figure shows the variation of static-pressure drop across the hot gas

injector as a fraction of the static pressure of the combustor exhaust with over-all equivalence ratio for two fuel flows. The static-pressure drop is defined as the pressure difference between station D-D of the primary combustor and the discharge face of the afterburner flameholder. The afterburner static pressure was actually measured at station E-E and was converted to the static pressure at the flameholder discharge face by correcting for the flameholder area blockage (neglecting the friction pressure loss between the two stations). The static-pressure drop for the two configurations was about the same, ranging from 1 to 4 percent.

Resonating Combustion

Resonating combustion, which resulted in combustor pressure fluctuations and exhaust temperature variations, was encountered with some combustor and afterburner designs. A detailed investigation of the factors involved in the resonating combustion was not attempted. It was felt that this particular mode of combustion was the result of a coupling that existed between the heat-release rate and the inlet mass flow. Accordingly, two approaches were used to control the resonating combustion; first, the pressure loss across the primary air injector was increased, and second, the heat-release rate was altered in both the primary combustor and afterburner by decreasing the equivalence ratio in the former and increasing the equivalence ratio in the latter. These changes resulted in satisfactory combustor operation free of resonance. It is interesting to note that the low-pressure-loss afterburner configurations were free of resonance when the afterburner was operated at an equivalence ratio near 1.

CONCLUDING REMARKS

Results of this investigation indicate, in general, that fuel-rich combustors can be designed with low pressure loss to give high combustion efficiency over a wide range of equivalence ratio. Stability limits observed with some combustor designs suggest that particular attention should be given to the manner in which the fuel and air are mixed. Stable operation was obtained over a broad equivalence-ratio range when air was injected normal to the fuel stream. It is felt that combustor outlet-temperature profiles can be controlled with appropriate primary-combustor designs.

In addition, the results obtained suggest that low-pressure-loss afterburner flameholders can be designed to give stable and efficient operation over a wide range of afterburner equivalence ratio. To obtain uniform afterburner temperature profiles, the distribution of the fuel-rich primary exhaust had to be controlled. Two low-pressure-loss afterburner designs were evolved that provided this control, an open U-gutter

employing turning vanes and a punched-plate flameholder. Resonating combustion, which occurred with some low-pressure-loss designs, was eliminated when the heat-release rates in the primary combustor and the afterburner were altered; also, increasing the pressure loss across the primary-combustor air injector resulted in resonant-free combustion.

Lewis Flight Propulsion Laboratory
National Advisory Committee for Aeronautics
Cleveland, Ohio, March 26, 1958

REFERENCES

1. Rae, Randolph S.: Various Engine Cycles Using Hydrogen as a Working Fluid and as a Fuel. Paper presented at meeting Inst. Aero. Sci. (Cleveland), Mar. 14, 1957. (ASTIA No. AD 119631.)

2. Morris, James F.: Analysis for Turbojet Thrust Augmentation with Fuel-Rich Afterburning of Hydrogen, Diborane, and Hydrazine. NACA RM E57D22, 1957.

3. Breitwieser, Roland, and Morris, James F.: A Preliminary Analysis of Hydrogen-Rich Hypersonic Ramjet Operation. NACA RM E57H27, 1957.

4. English, Robert E., and Hauser, Cavour H.: Thermodynamic Properties of Products of Combustion of Hydrogen with Air for Temperatures of 600° to 4400° F. NACA RM E56G03, 1956.

5. Keenan, Joseph H., and Kaye, Joseph: Gas Tables. John Wiley & Sons, Inc., 1948.

6. Keenan, Joseph H., and Keyes, Frederick G.: Thermodynamic Properties of Steam. John Wiley & Sons, Inc., 1936.

TABLE I. - PRIMARY-COMBUSTOR TEST DATA

Run	Primary-combustor inlet static pressure, in. Hg abs	Air-injector inlet static pressure, in. Hg abs	Combustor inlet total temperature, °F		Fuel-flow rate, lb/hr	Primary airflow rate, lb/sec	Equivalence ratio	Mean combustor outlet temperature, °F	Mean temperature rise through combustor, °F	Combustion efficiency, percent	Air-injector static-pressure drop, percent	Combustor pressure loss, percent	Combustor inlet reference velocity, ft/sec
			Air	Fuel									
Flameholder model A													
1	35.0	34.0	82	60	151.7	0.153	8.19	[a]1226	1154	-----	----	----	80.4
2	32.9	34.8	82	72	141.2	.139	9.66	[a]1359	1282	-----	----	----	101.1
3	32.4	34.0	88	85	122.4	.130	8.94	[a]1461	1574	-----	----	----	92.1
4	31.9	37.0	88	84	101.8	.0942	10.27	1316	1230	103.9	13.8	0.28	75.8
5	31.9	37.0	83	89	102.4	.0958	10.16	1063	977	80.7	13.8	.28	76.8
6	31.3	34.0	84	86	101.4	.0854	14.75	914	829	83.9	7.9	.22	72.6
7	31.5	32.5	84	84	100.6	.0856	20.96	724	640	99.0	3.1	.20	68.4
8	31.6	40.5	84	82	105.0	.1246	8.01	1511	1428	99.4	21.0	.34	82.7
9	31.4	40.0	84	77	102.3	.0953	10.21	1283	1202	101.0	14.0	.25	76.5
10	33.8	42.2	86	80	199.2	.1268	14.94	869	786	90.2	19.9	.62	130.7
11	32.8	36.0	86	58	205.4	.0746	26.19	551	459	88.9	8.9	.61	125.7
12	31.4	35.0	85	78	99.4	.0947	9.98	1233	1151	94.7	10.3	.22	74.8
13	31.4	35.0	85	78	99.4	.0942	9.98	939	857	89.7	10.3	.22	74.8
14	31.4	34.8	87	79	98.1	.1890	9.90	1007	924	74.8	10.3	.22	74.1
15	34.1	46.0	87	102	203.4	.1889	10.24	1250	1135	84.8	26.3	.88	148.4
16	34.9	40.0	91	86	209.8	.1245	16.03	643	554	67.2	13.5	.70	133.5
17	32.5	35.8	92	89	197.9	.0953	19.75	506	415	60.4	9.8	.64	132.6
18	31.2	34.8	92	85	102.7	.0950	10.28	954	865	72.1	10.3	.20	78.4
19	33.2	40.5	93	72	208.0	.1458	13.57	710	627	66.3	18.5	.72	139.4
20	33.3	41.5	96	83	146.8	.0921	15.16	824	734	85.6	----	----	-----
21	36.5	39.0	96	80	144.8	.0559	24.64	547	459	83.1	4.0	.24	83.3
22	34.9	40.0	98	75	142.9	.1261	10.78	1246	1159	102.2	----	----	-----
23	31.2	34.9	89	93	99.8	.0934	10.16	1240	1148	95.7	9.7	.25	77.1
24	37.9	49.0	88	87	202.7	.1906	10.12	1155	1067	88.4	22.0	.70	127.9
25	35.2	47.0	90	77	205.8	.1885	10.23	1177	1088	91.7	24.0	.80	136.2
26	32.0	35.0	91	72	102.3	.0958	10.37	983	901	76.1	9.7	.24	74.5
27	34.4	46.0	91	78	198.4	.1883	10.02	1200	1116	92.1	26.0	.81	136.5
28	32.8	36.0	91	69	206.6	.0935	21.01	538	458	71.8	8.0	.51	131.8
29	33.9	37.1	90	66	211.0	.0936	21.43	551	473	75.7	9.2	.49	129.2
30	35.3	38.5	85	103	100.9	.0957	10.03	1098	1004	81.8	8.3	.21	70.0
31	51.5	60.0	86	101	200.6	.1919	9.94	1108	1014	82.2	14.3	.39	95.3
32	33.4	36.7	88	95	100.8	.0952	10.07	1057	965	79.1	9.2	.21	73.1
33	34.5	40.0	88	91	101.0	.1267	7.58	1490	1400	93.1	14.3	.23	74.9
34	45.0	54.5	87	89	209.2	.1886	10.55	1022	934	79.5	17.4	.45	110.6
35	32.4	36.5	89	83	102.1	.0952	10.20	1307	1221	102.8	10.1	.27	74.8
36	39.2	49.0	89	70	205.9	.1878	10.43	1170	1090	93.2	21.4	.64	121.8
37	35.7	38.8	83	84	104.6	.0952	10.45	948	884	72.8	8.2	.20	69.2
38	35.5	38.7	84	72	103.2	.0950	10.33	1165	1086	91.7	8.0	.23	67.6
39	36.7	42.5	87	87	99.1	.1312	7.19	1659	1564	100.7	15.6	.22	67.7
40	34.8	35.0	86	84	108.3	.0482	20.76	577	502	77.9	2.6	.12	62.8
Flameholder model B													
41	32.2	50.0	88	71	136.9	0.0830	15.69	866	746	94.8	35.6	1.17	92.1
42	30.7	54.5	86	96	99.5	.0960	9.86	1296	1205	98.0	44.0	.83	78.9
43	33.7	80.0	90	82	214.8	.1490	13.71	905	817	87.2	55.4	2.54	143.5
44	33.7	53.5	89	81	204.8	.0913	21.33	581	296	46.1	36.6	1.69	129.5
45	30.8	42.0	89	73	102.1	.0625	15.54	896	814	97.3	26.7	.57	72.5
46	31.2	84.0	86	68	103.2	.1193	8.25	1379	1225	92.3	51.3	.89	82.6
47	31.2	70.5	86	65	107.3	.1338	7.65	1433	1357	90.9	55.7	1.09	87.1
Flameholder model C													
48	31.0	33.5	82	84	100.1	0.0962	9.89	1296	1203	98.2	6.6	1.43	77.1
49	30.8	32.0	84	82	101.3	.0641	15.02	947	864	99.8	3.1	.98	73.1
50	30.8	31.2	84	81	100.4	.0481	19.86	748	665	98.2	1.9	.72	69.9
51	30.6	31.0	86	79	101.1	.0398	24.17	631	548	97.0	1.3	.61	69.3
52	34.9	42.0	87	74	208.0	.1913	10.34	1290	1210	102.8	17.1	3.96	139.3
53	32.9	37.0	85	88	202.5	.1264	15.24	954	867	101.2	10.8	2.51	137.8
54	32.8	35.0	84	87	205.7	.0950	20.60	-----	-----	Blowout	7.9	1.98	135.3
55	32.5	38.0	85	81	206.8	.0971	20.26	----	----	Blowout	5.0	2.25	136.2
56	32.9	36.0	84	78	205.0	.1101	17.71	804	723	96.2	9.4	2.46	135.1
57	31.1	33.4	84	75	102.3	.0948	10.26	1264	1185	99.9	7.2	1.44	76.9
58	31.4	35.2	85	75	100.7	.1256	7.62	1583	1483	99.8	10.5	1.73	80.0
59	30.5	31.0	84	72	101.0	.0469	20.46	724	646	98.5	1.9	.62	69.7
60	36.1	47.0	87	71	208.0	.2446	8.01	1553	1474	103.0	23.4	4.35	140.0
61	31.1	34.4	87	63	103.3	.1129	8.70	1402	1327	98.6	7.4	1.71	81.5
Flameholder model D													
62	31.0	31.8	83	82	101.8	0.0951	10.2	1220	1137	95.0	2.2	0.48	77.7
63	30.5	31.0	83	80	102.0	.0630	15.4	912	830	98.0	1.0	.27	73.8
64	30.6	30.9	83	77	102.8	.0478	20.4	759	679	103.1	.6	.20	71.3
65	30.5	30.8	85	76	102.8	.0388	25.1	634	554	101.7	.5	.14	69.9
66	31.6	33.0	83	74	101.9	.1328	7.3	1566	1488	98.6	3.9	.76	81.0
67	32.8	33.5	85	75	205.7	.0956	20.3	643	563	84.8	2.1	.57	131.6
68	32.5	32.9	83	71	204.7	.0759	25.6	566	490	91.6	1.4	.40	129.5
69	33.4	34.2	85	68	204.3	.1254	15.5	778	702	85.4	3.4	.80	132.3
70	34.5	36.9	86	85	207.9	.1901	10.4	1103	1026	87.4	6.7	1.57	138.6
71	30.9	32.0	83	84	103.5	.0956	10.3	1195	1121	94.8	2.3	.48	77.0
72	31.0	32.0	74	70	102.4	.0963	10.1	1257	1165	96.8	2.2	.62	76.6
73	30.6	31.0	75	70	103.0	.0476	20.6	734	661	100.9	.5	.23	70.5
74	33.1	33.5	73	66	205.2	.0981	20.3	667	598	90.0	1.9	.81	129.0
75	34.8	36.9	74	60	207.4	.1905	10.4	1169	1102	93.4	6.0	1.91	135.5

[a]Single-point readings.

[redacted]

TABLE II. - AFTERBURNER TEST DATA

Run	Afterburner inlet static pressure, in. Hg abs	Afterburner inlet temperature (air), °F	Afterburner airflow rate, lb/sec	Over-all equivalence ratio	Afterburner reference velocity, ft/sec	Afterburner combustion efficiency, percent
Afterburner flameholder configuration 1						
1	34.0	90	6.92	0.159	84.7	----
Afterburner flameholder configuration 2						
2	34.8	83	6.62	0.184	78.1	----
Afterburner flameholder configuration 3						
3	34.0	92	7.32	0.142	89.9	----
Afterburner flameholder configuration 4						
4	37.0	92	4.362	0.2173	140	89.2
5	36.0	85	4.185	.2275	136	80.4
6	34.0	86	3.178	.2973	110	99.5
7	33.5	85	3.049	.3091	107	97.5
8	33.0	86	2.778	.3440	99	93.0
9	33.0	86	2.731	.3442	97	----
10	37.1	86	3.941	.4657	125	92.7
11	34.5	89	2.824	.6738	97	91.3
15	31.8	89	2.086	.8502	78	87.0
16	34.5	91	4.440	.4371	153	90.9
17	31.8	92	2.189	.8240	82	95.3
18	30.8	91	2.187	.4280	85	95.3
19	31.8	92	2.090	.8846	79	94.1
21	30.8	95	1.759	.5125	68	95.2
24	38.0	95	7.389	.2543	230	91.9
25A	33.5	95	7.551	.5180	268	97.7
25B	33.5	95	7.551	.5180	268	94.4
26	32.0	94	3.637	.2606	135	84.4
27	32.0	95	2.147	.8079	80	93.8
28	32.0	94	2.145	.8778	80	94.2
29	33.5	93	3.675	.5324	130	94.5
Afterburner flameholder configuration 5						
30	37.7	86	3.697	0.2529	115	97.5
31	55.3	87	6.331	.2925	135	91.3
32	34.0	87	2.224	.4134	77	100.5
33	34.5	88	2.278	.3993	78	97.6
34	46.5	89	4.355	.4378	111	90.2
35	31.8	89	1.073	.8314	40	93.4
36	37.8	89	2.149	.8379	67	92.8
37	38.0	85	3.575	.2711	110	92.8
38	37.9	88	3.592	.2661	111	97.4
39	38.5	89	3.597	.2528	110	93.6
40	37.0	88	3.694	.2675	118	95.4

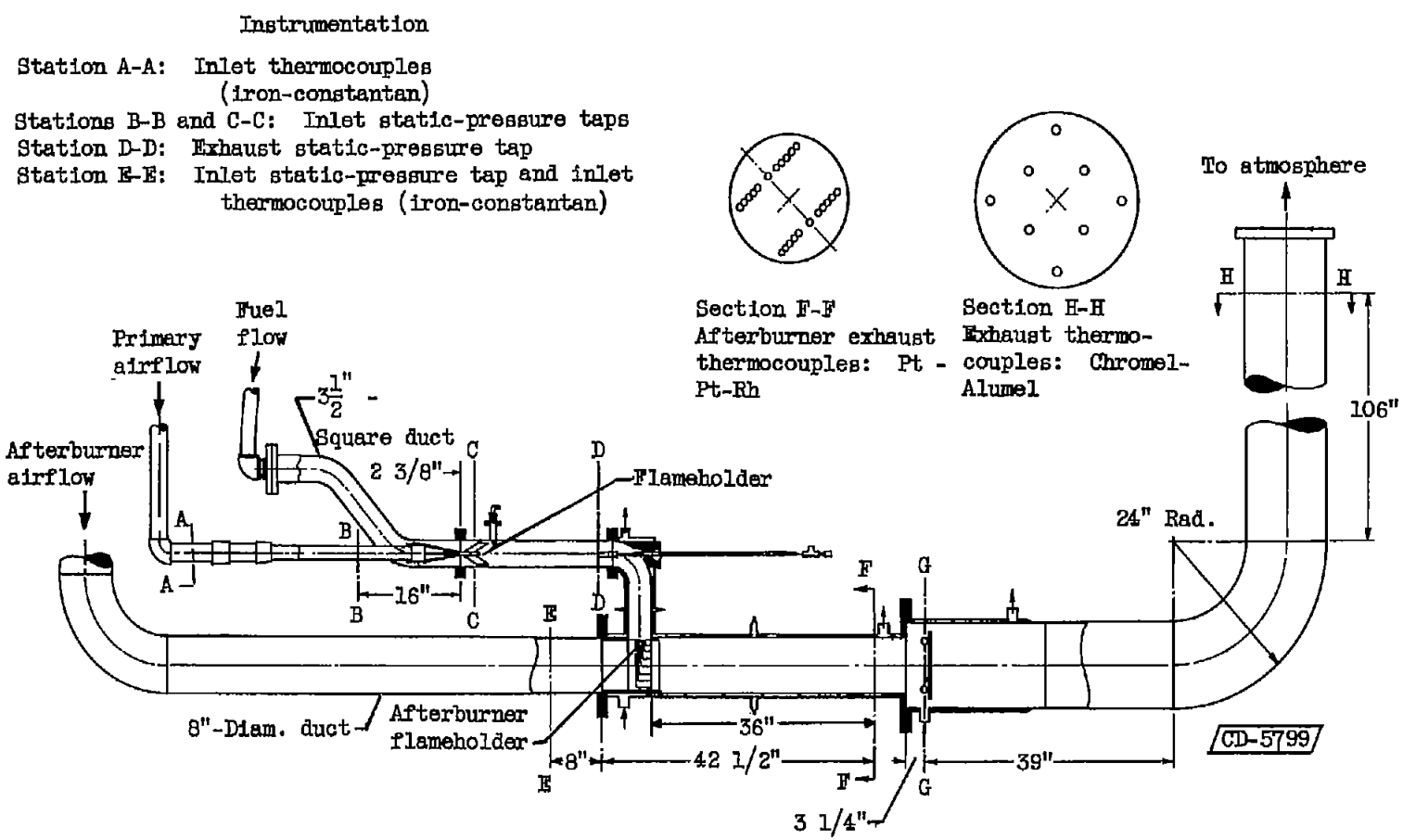

(a) Instrumentation detail.

Figure 1. - Combustor and afterburner installation showing location of temperature- and pressure-measuring instruments in instrumentation planes.

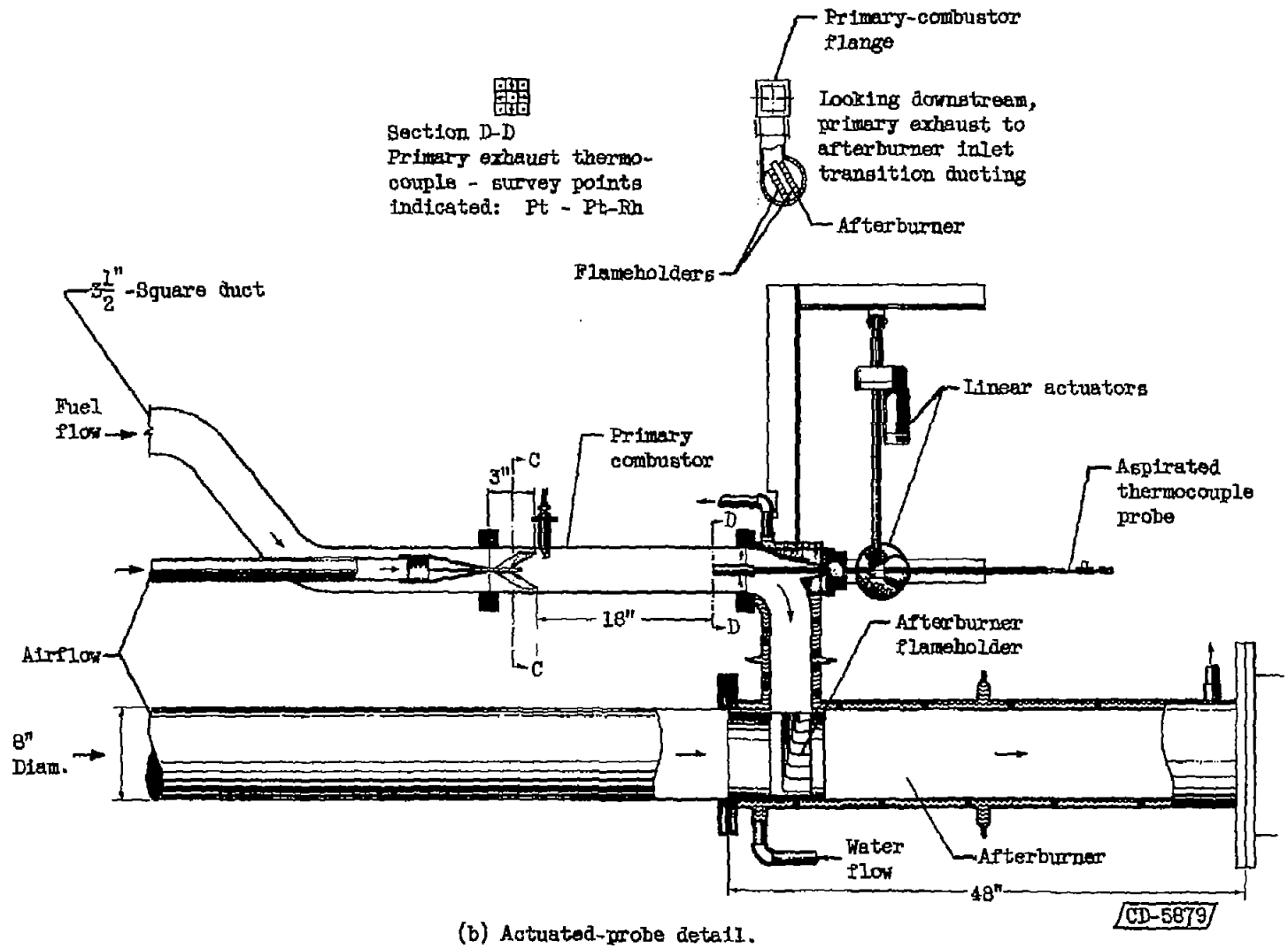

(b) Actuated-probe detail.

Figure 1. - Concluded. Combustor and afterburner installation showing location of temperature- and pressure-measuring instruments in instrumentation planes.

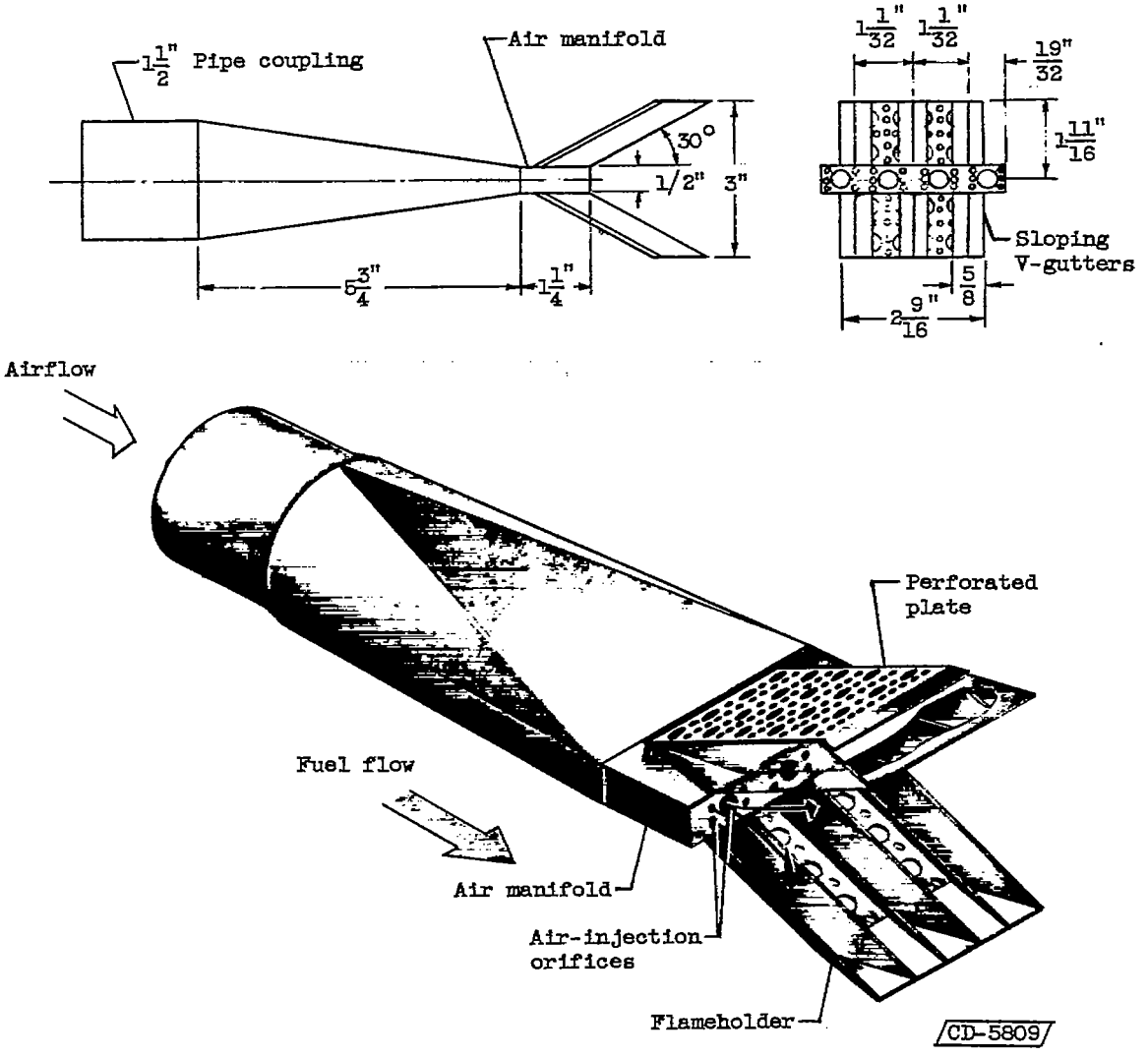

(a) Primary-combustor model A.

Figure 2. - Cutaway views of primary-combustor flameholders.

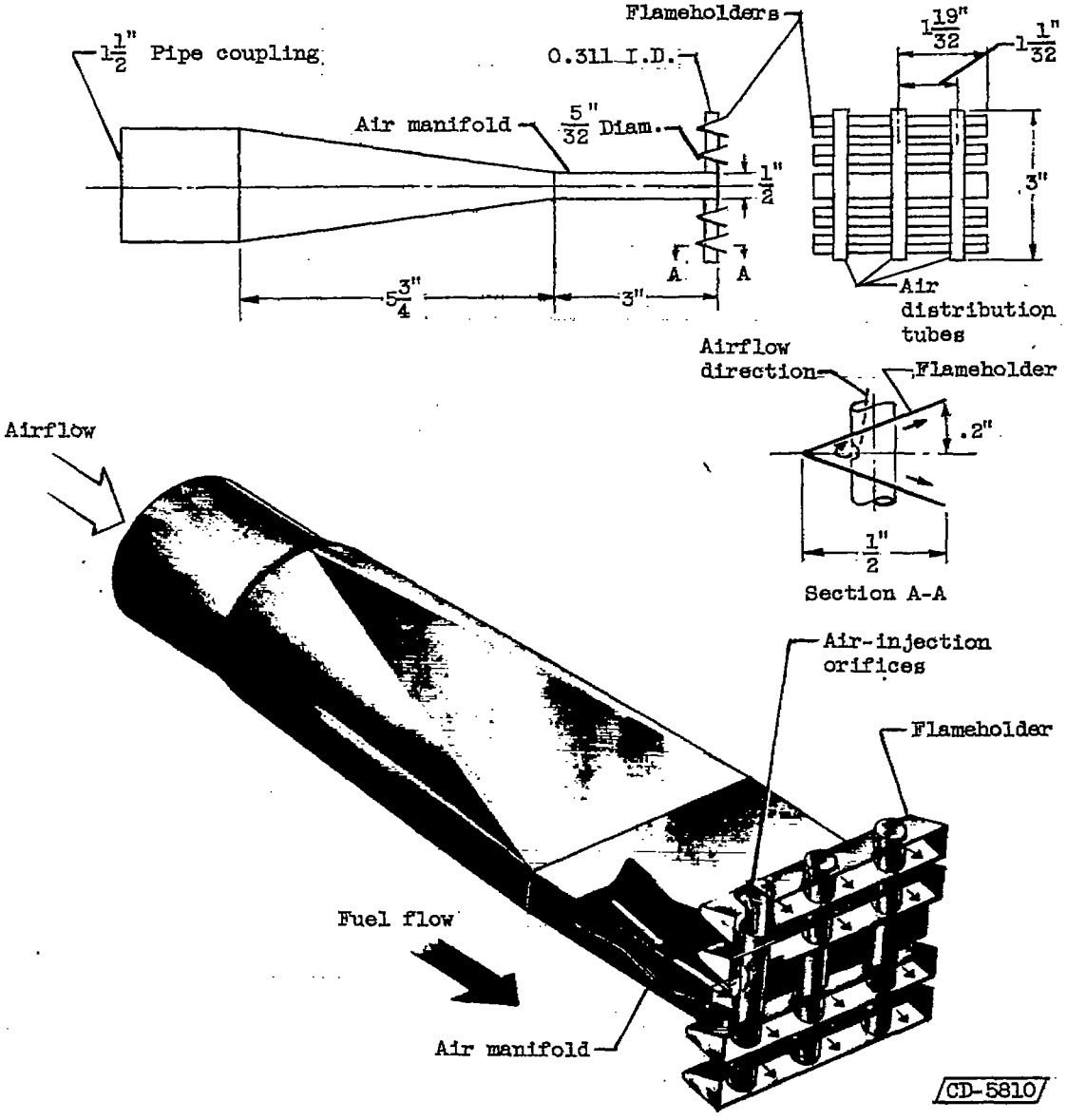

(b) Primary-combustor model B.

Figure 2. - Continued. Cutaway views of primary-combustor flameholders.

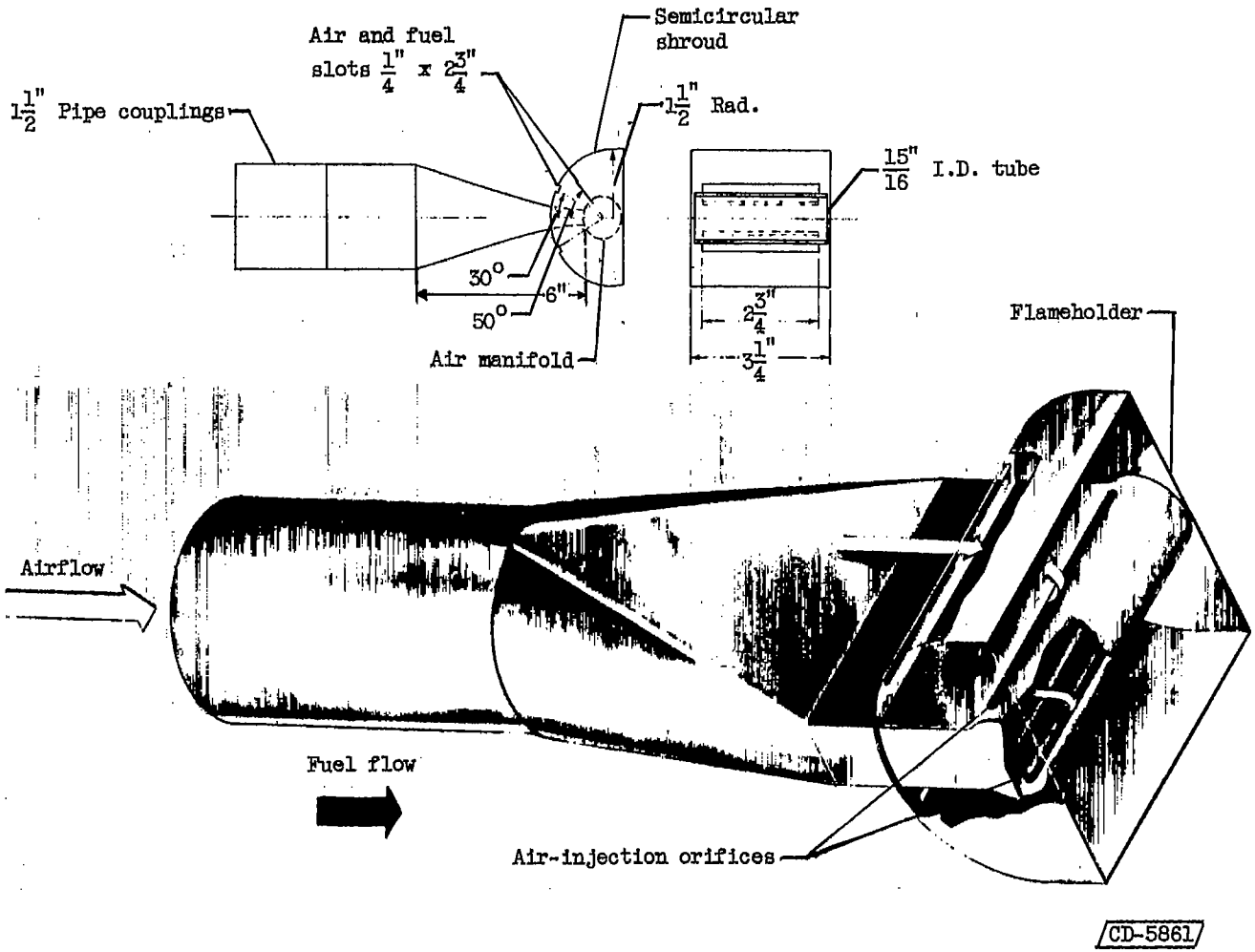

(c) Primary-combustor model C.

Figure 2. - Continued. Cutaway views of primary-combustor flameholders.

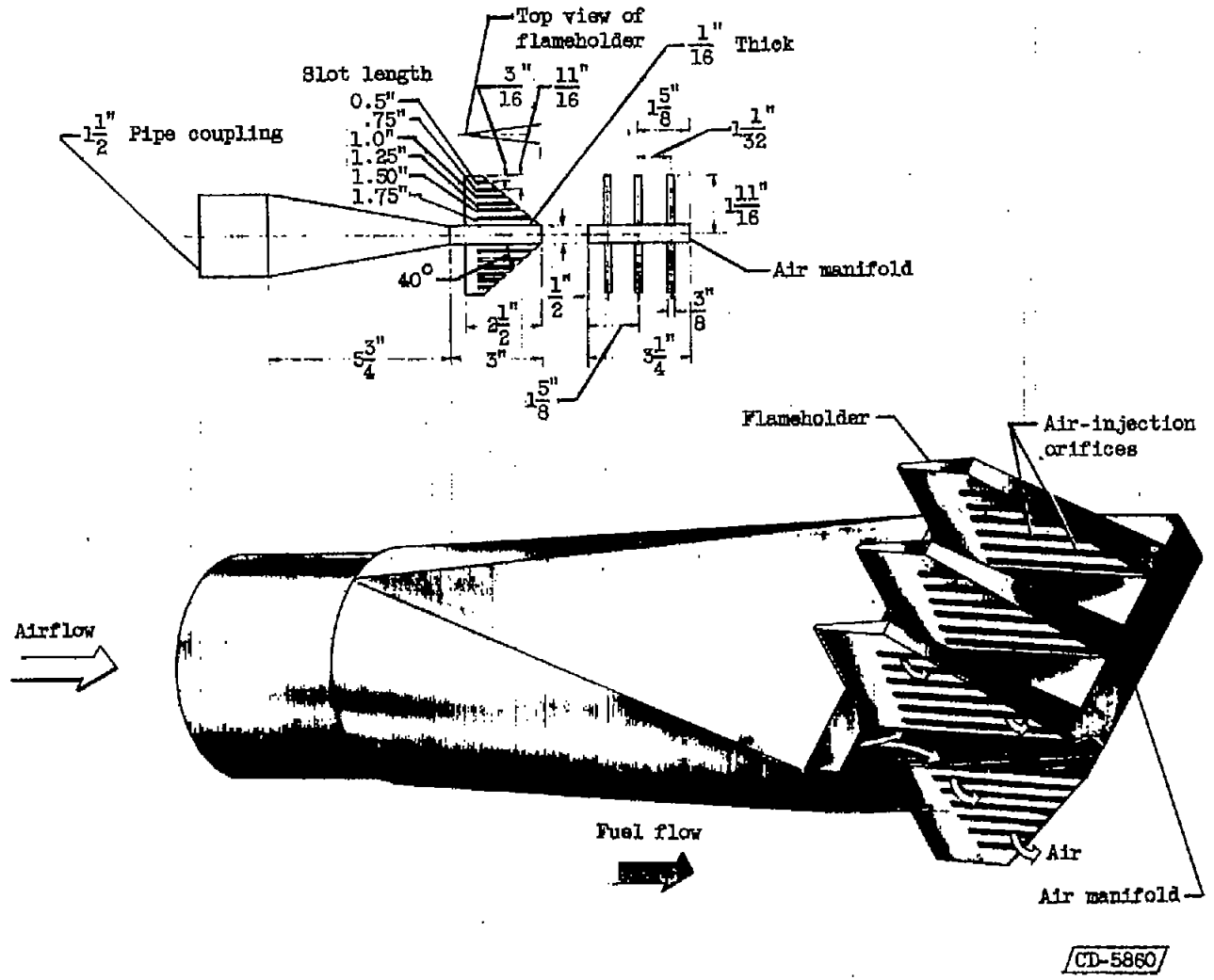

(d) Primary-combustor model D.

Figure 2. - Concluded. Cutaway views of primary-combustor flameholders.

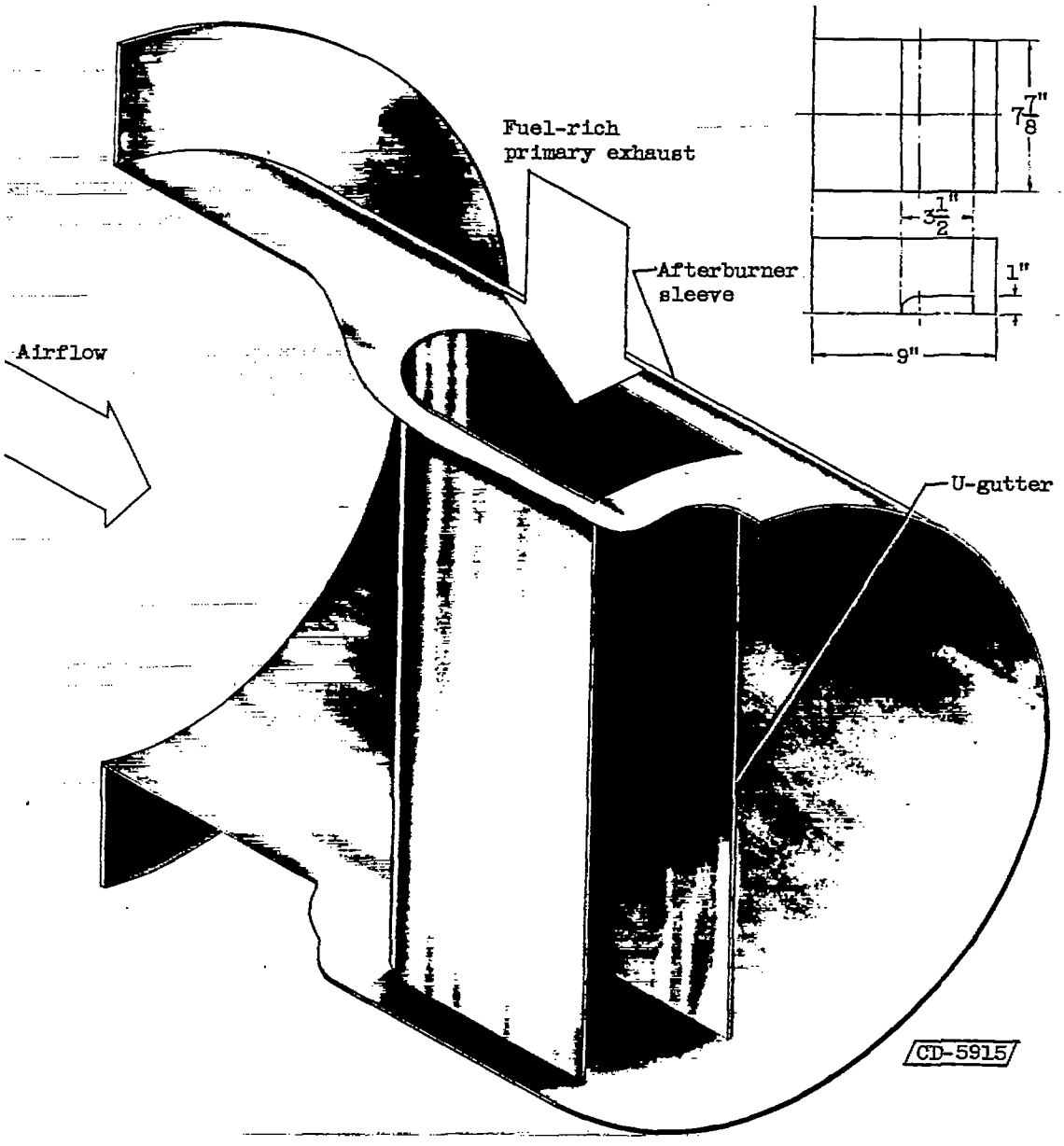

(a) Flameholder configuration 1.

Figure 3. - Cutaway views of afterburner flameholders.

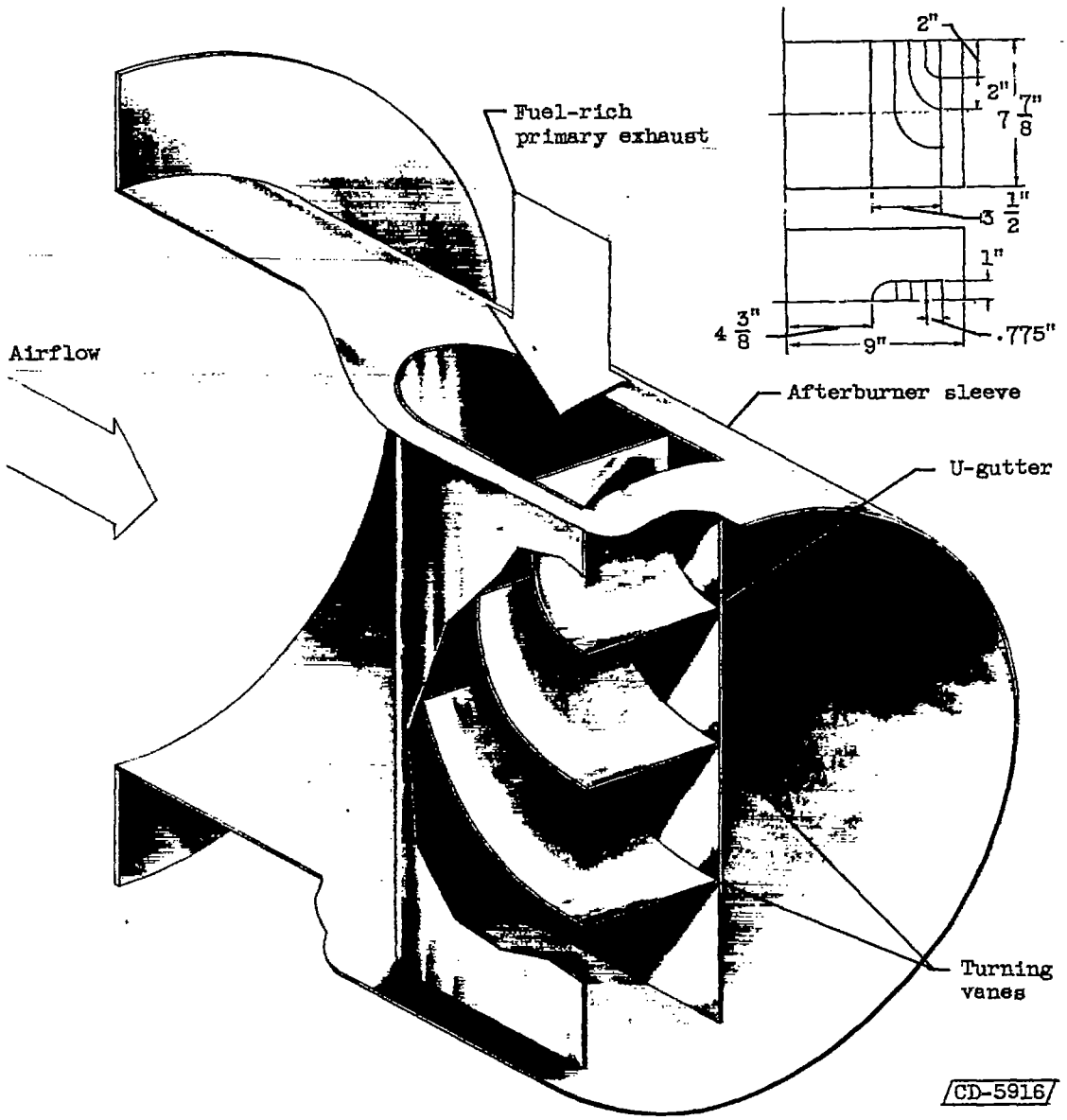

(b) Flameholder configuration 2.

Figure 3. - Continued. Cutaway views of afterburner flameholders.

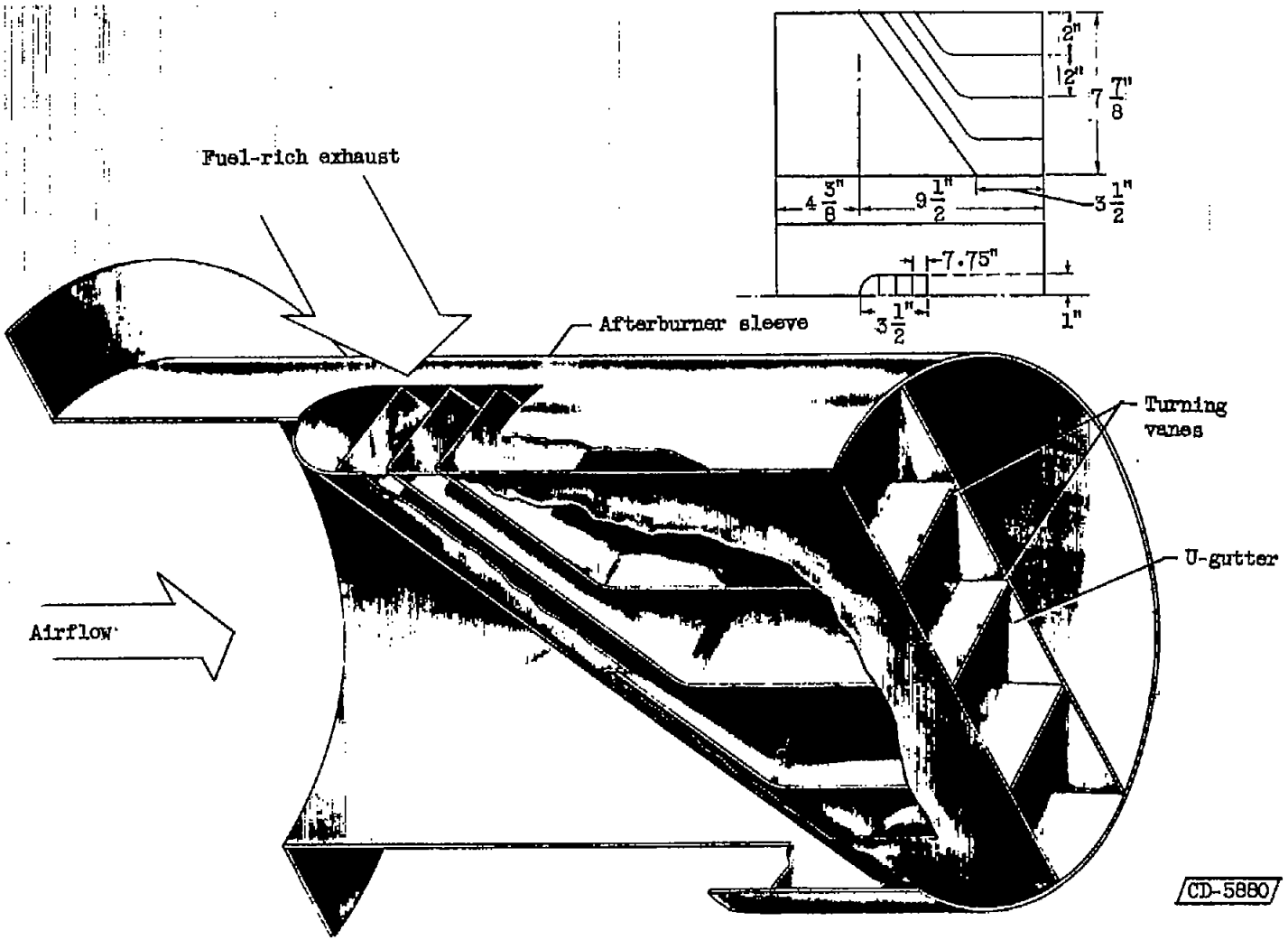

(c) Flameholder configuration 3.

Figure 3. - Continued. Cutaway views of afterburner flameholders.

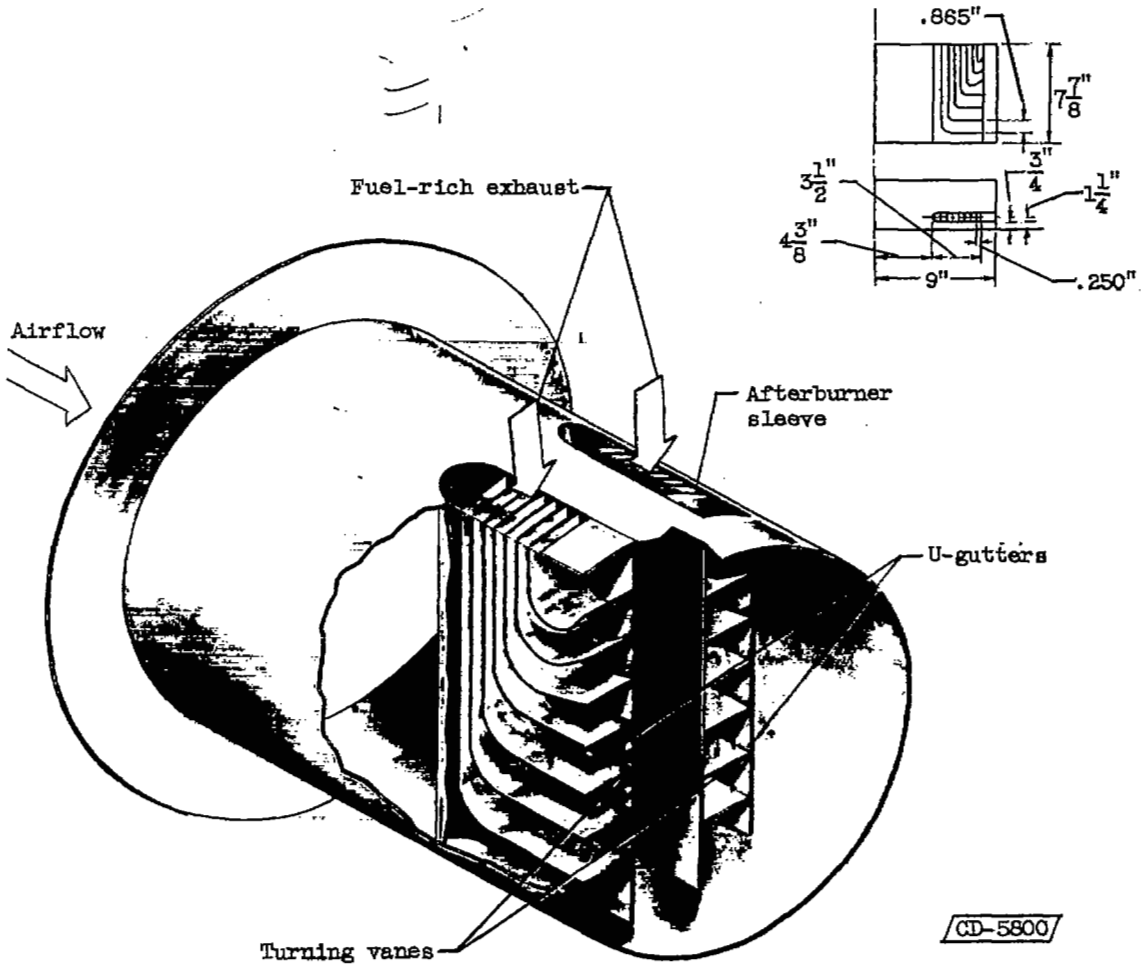

(d) Flameholder configuration 4.

Figure 3. - Concluded. Cutaway views of afterburner flameholders.

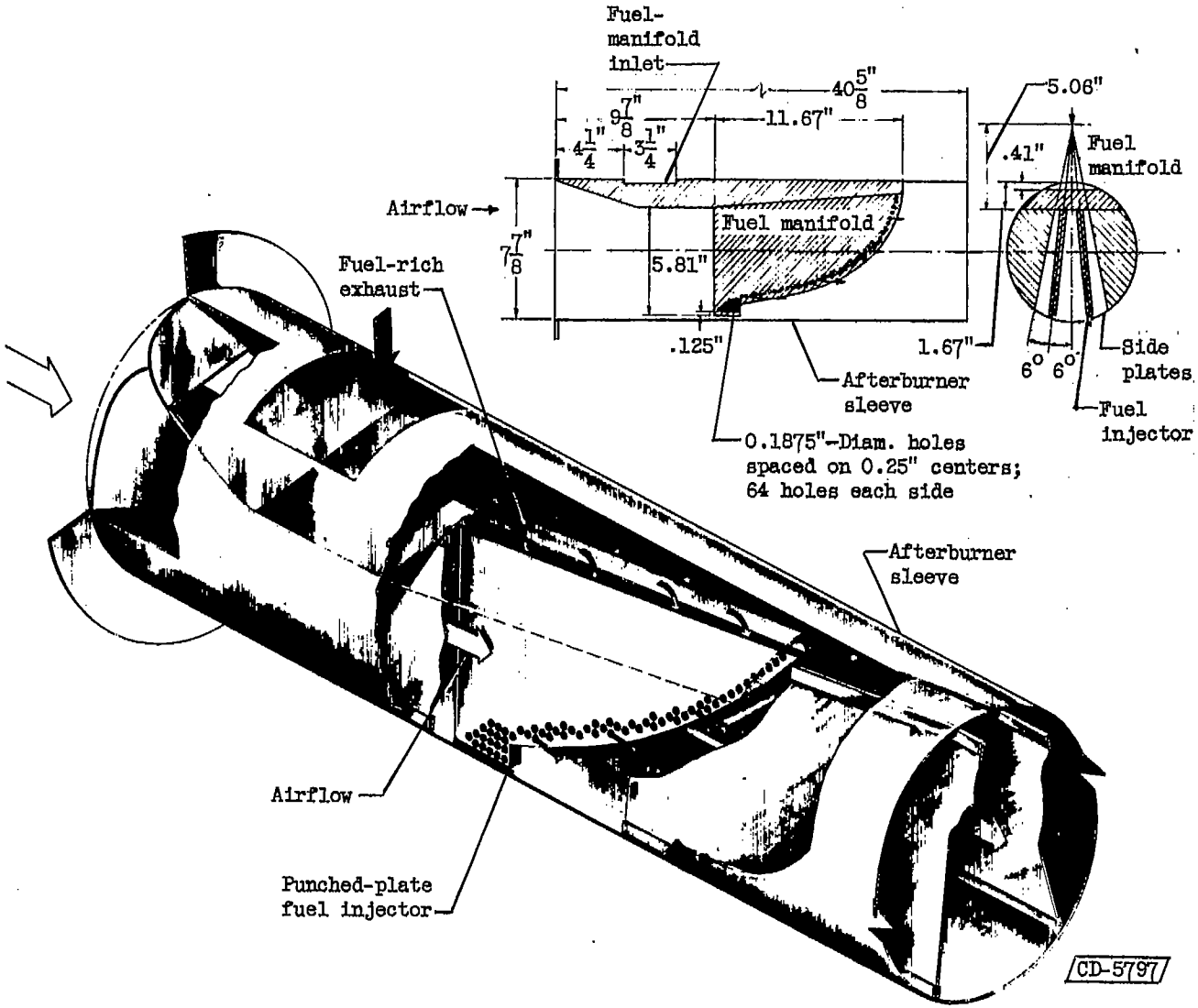

Figure 4. - Cutaway view of afterburner flameholder configuration 5.

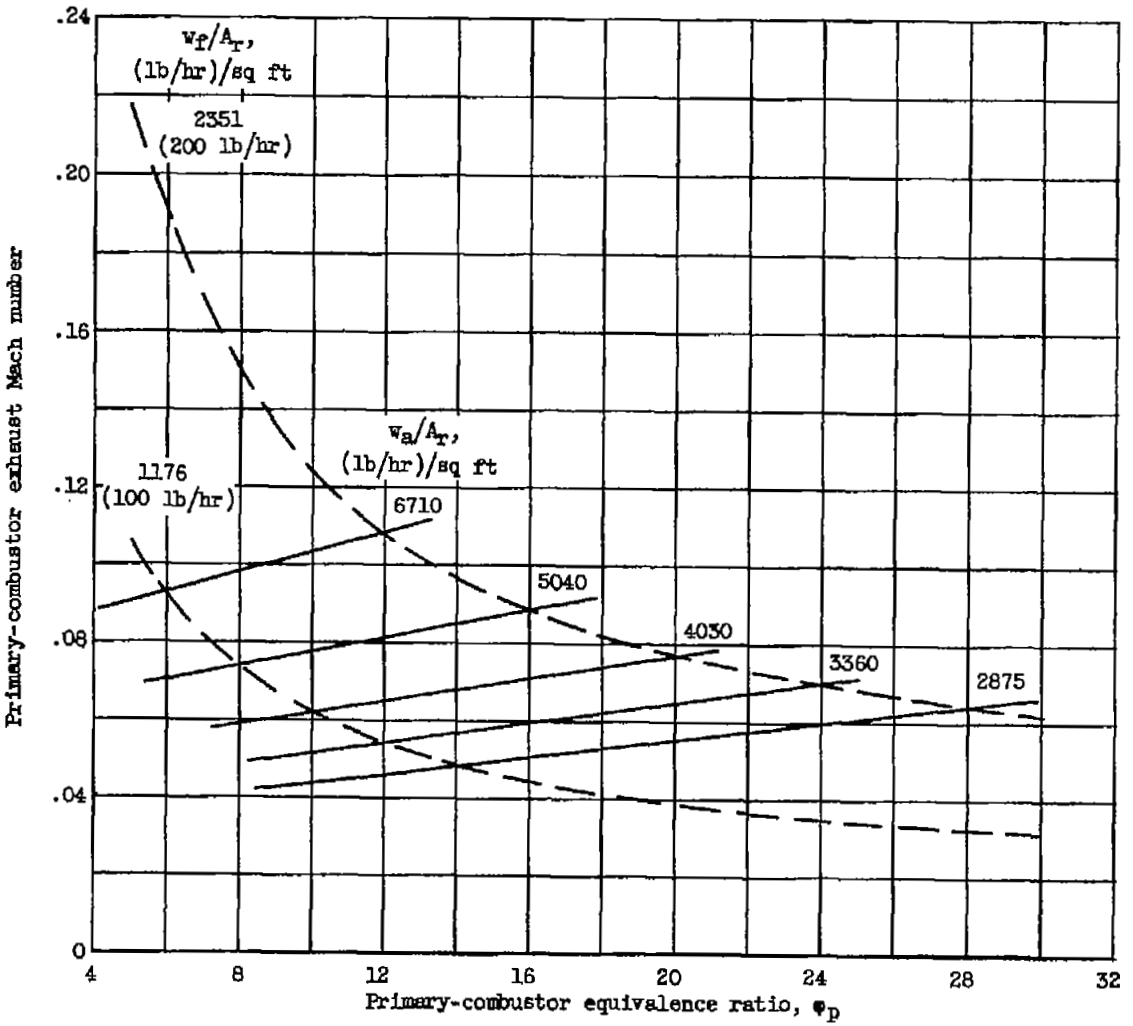

Figure 5. - Variation of primary-combustor exhaust Mach number with primary-combustor equivalence ratio. Inlet total pressure, 30 inches of mercury absolute; inlet temperature, 80° F; combustion efficiency, 100 percent; combustor cross-sectional area, 12.25 square inches.

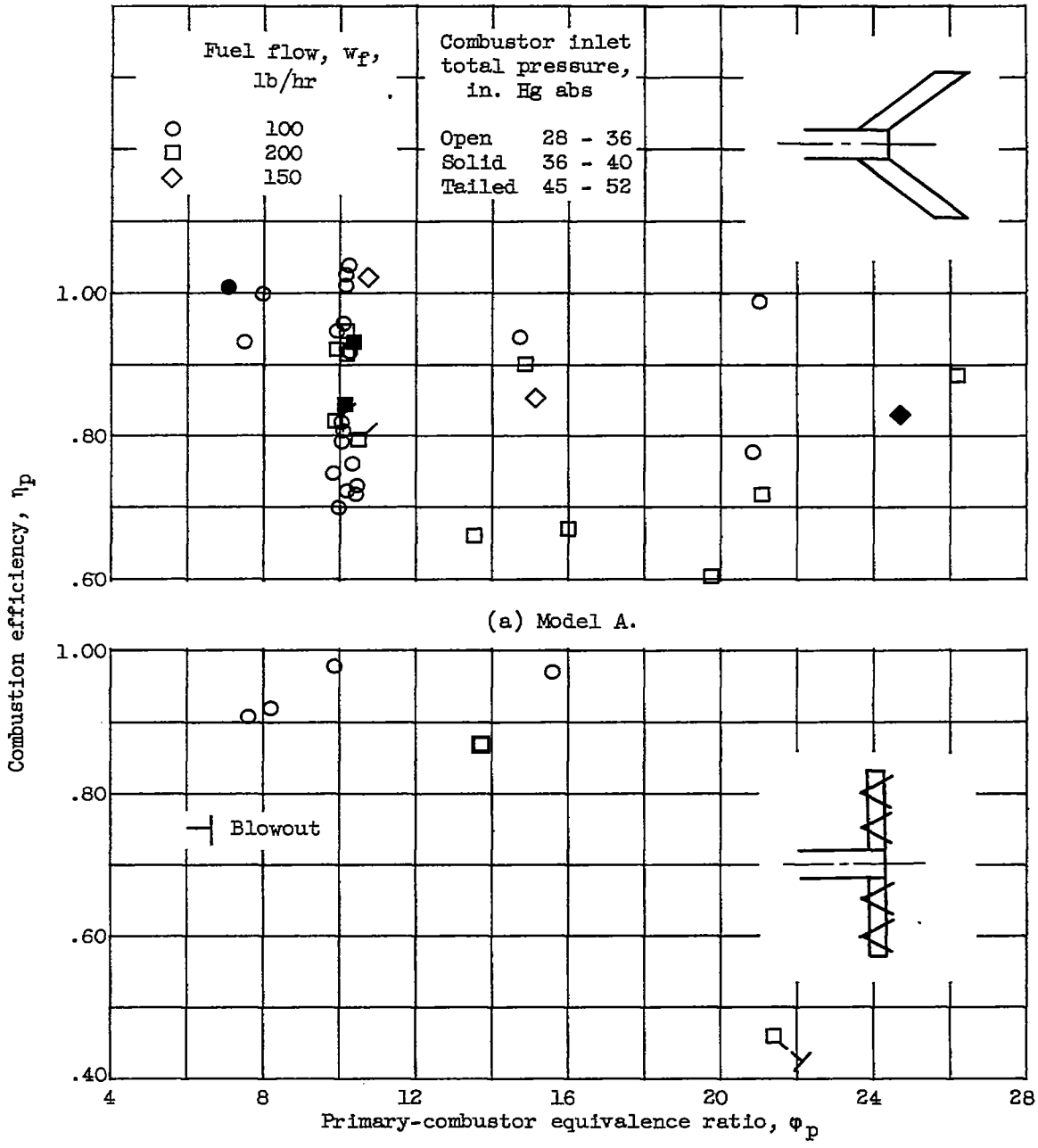

(b) Model B. Combustor inlet total pressure, approximately 33 inches of mercury absolute.

Figure 6. - Variation in combustion efficiency with primary-combustor equivalence ratio for four primary-combustor configurations. Inlet-air temperature, approximately 80° F.

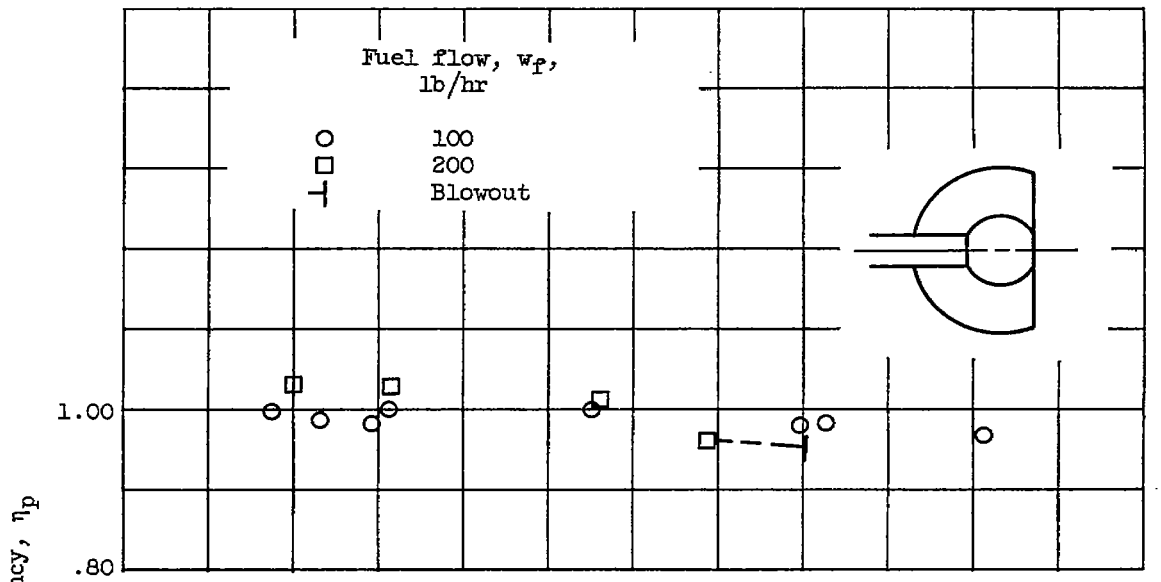

(c) Model C. Combustor inlet total pressure, approximately 33 inches of mercury absolute.

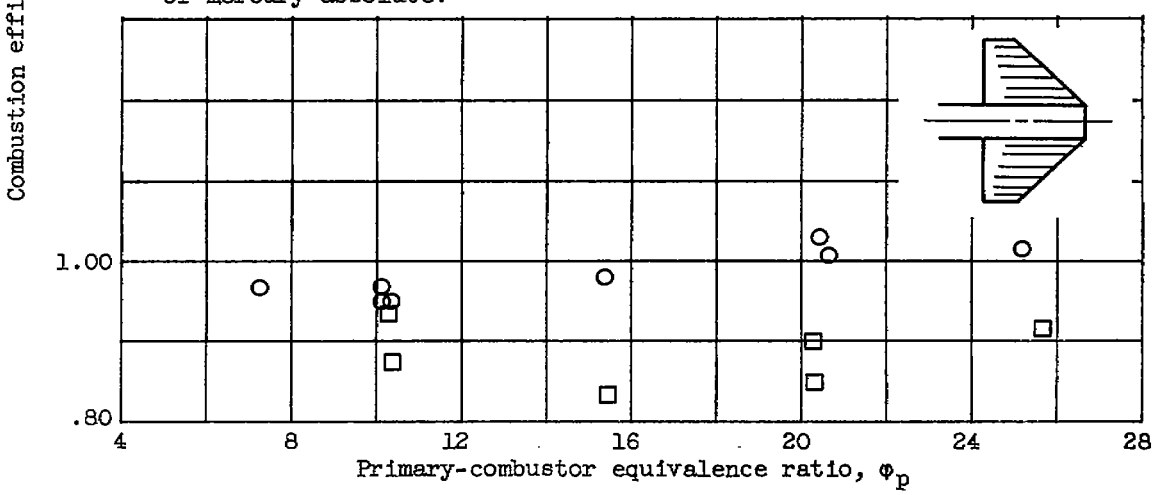

(d) Model D. Combustor inlet total pressure, approximately 33 inches of mercury absolute.

Figure 6. - Concluded. Variation in combustion efficiency with primary-combustor equivalence ratio for four primary-combustor configurations. Inlet-air temperature, approximately 80° F.

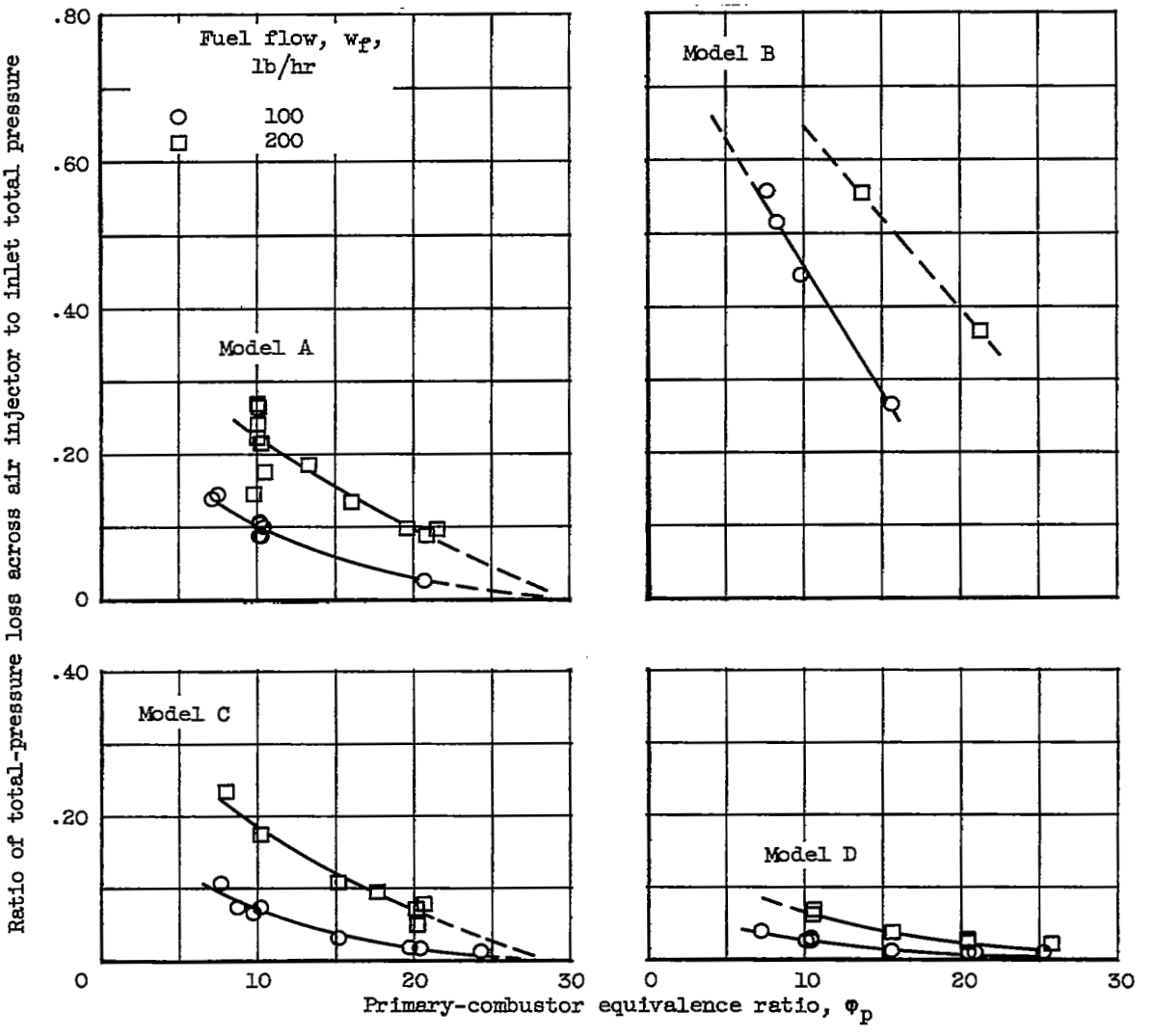

Figure 7. - Variation of air-injector pressure loss with primary-combustor equivalence ratio for various flameholder models. Inlet-air temperature, 80° F.

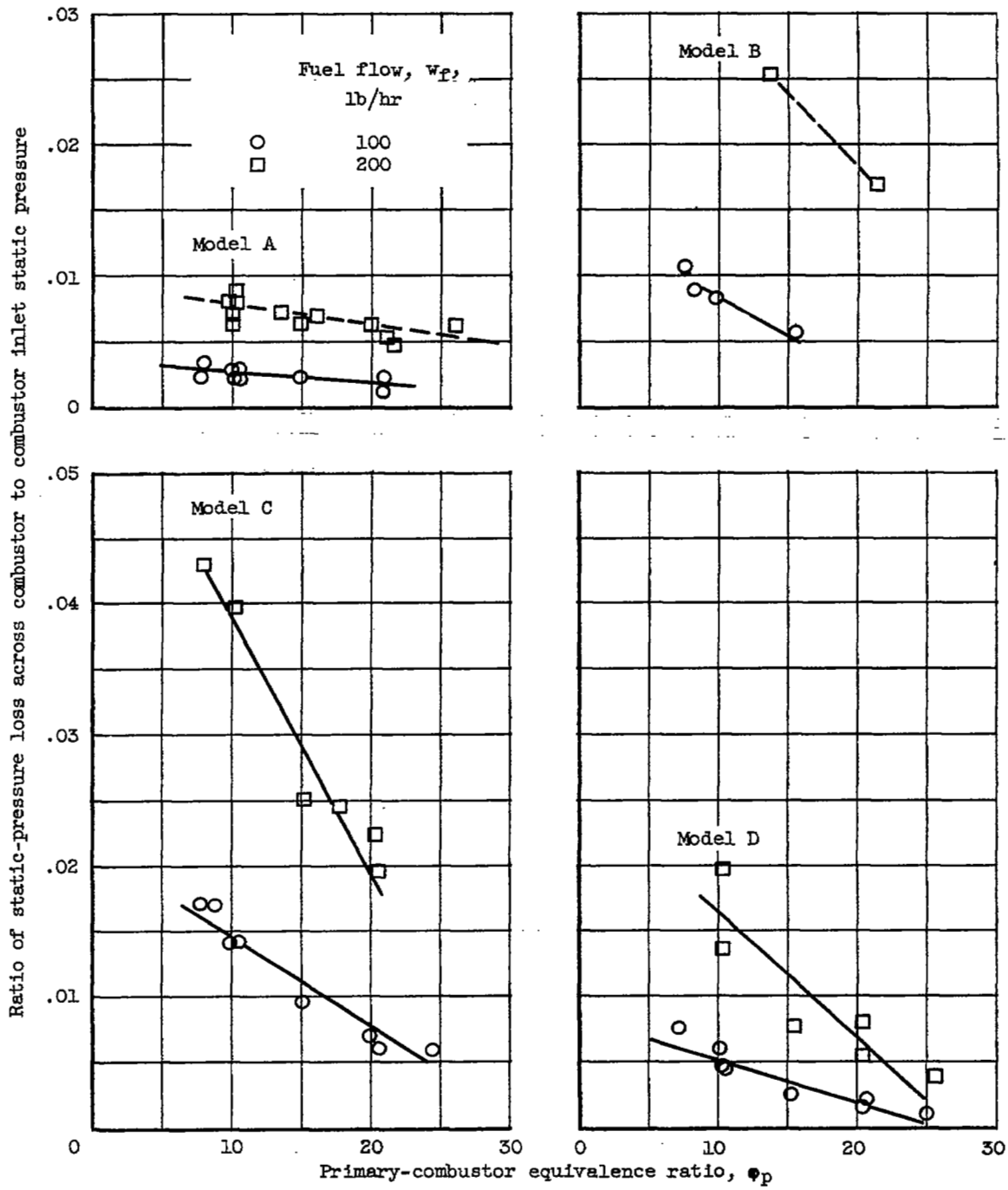

Figure 8. - Effect of various flameholder models on combustor pressure loss. Inlet-air temperature, 80° F.

CK-5

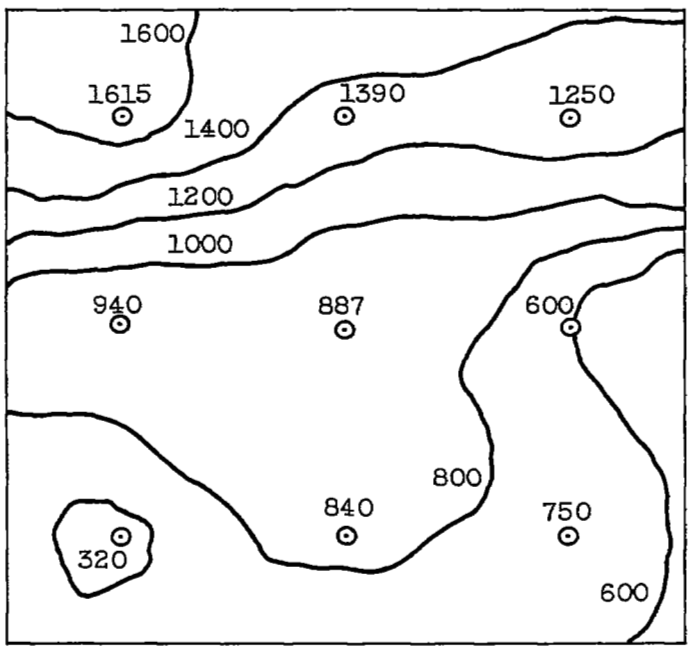

(a) Primary-combustor model A. Combustor inlet-air pressure, 31.2 inches of mercury absolute; inlet-air temperature, 80° F; inlet reference velocity, 78 feet per second; average outlet temperature, 954° F.

Figure 9. - Temperature pattern at combustor outlet (°F). Equivalence ratio, approximately 10; fuel-flow rate, 100 pounds per hour.

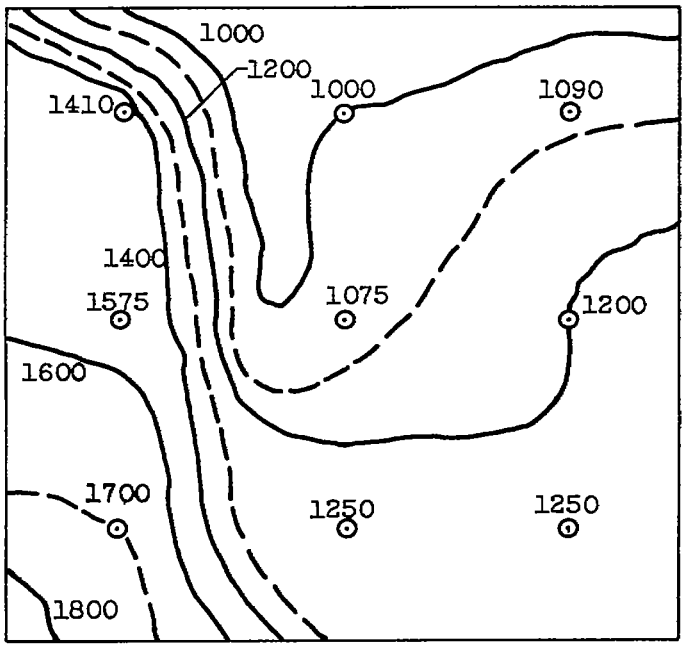

(b) Primary-combustor model A. Combustor inlet-air pressure, 31.4 inches of mercury absolute; inlet-air temperature, 80° F; inlet reference velocity, 77 feet per second; average outlet temperature, 1283° F.

Figure 9. - Continued. Temperature pattern at combustor outlet (°F). Equivalence ratio, approximately 10; fuel-flow rate, 100 pounds per hour.

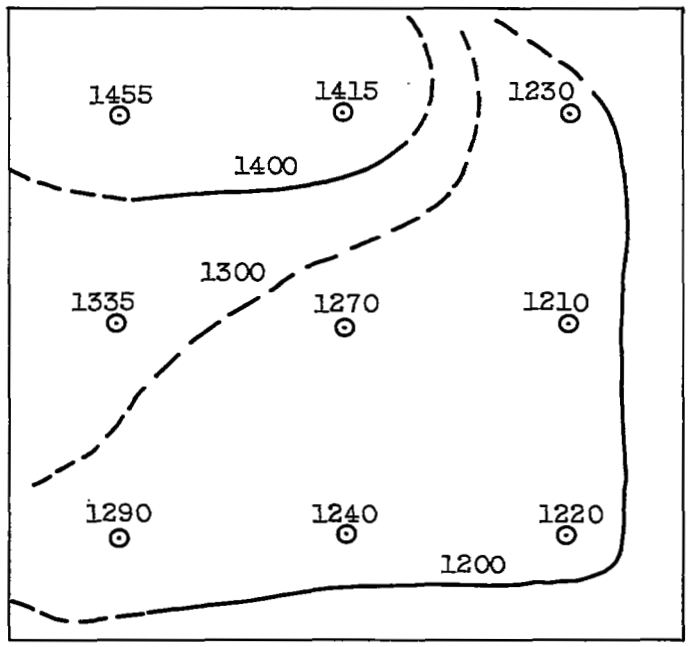

(c) Primary-combustor model B. Combustor inlet-air pressure, 30.7 inches of mercury absolute; inlet-air temperature, 85° F; inlet reference velocity, 79 feet per second; average outlet temperature, 1296° F.

Figure 9. - Continued. Temperature pattern at combustor outlet (°F). Equivalence ratio, approximately 10; fuel-flow rate, 100 pounds per hour.

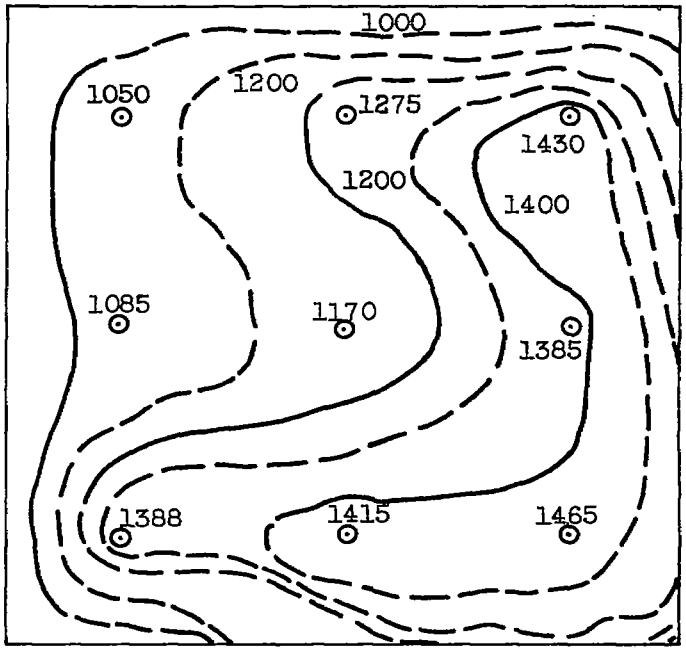

(d) Primary-combustor model C. Combustor inlet-air pressure, 31 inches of mercury absolute; inlet-air temperature, 82° F; inlet reference velocity, 77 feet per second; average outlet temperature, 1296° F.

Figure 9. - Continued. Temperature pattern at combustor outlet (°F). Equivalence ratio, approximately 10; fuel-flow rate, 100 pounds per hour.

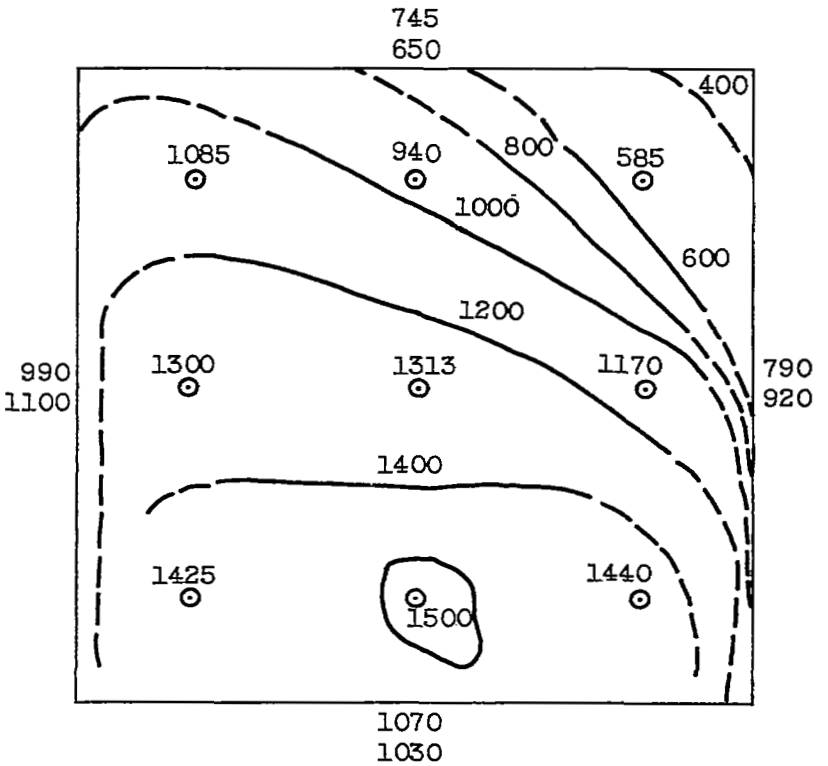

(e) Primary-combustor model D. Combustor inlet-air pressure, 30.9 inches of mercury absolute; inlet-air temperature, 83° F; inlet reference velocity, 77 feet per second; average outlet temperature 1195° F.

Figure 9. - Concluded. Temperature pattern at combustor outlet (°F). Equivalence ratio, approximately 10; fuel-flow rate, 100 pounds per hour.

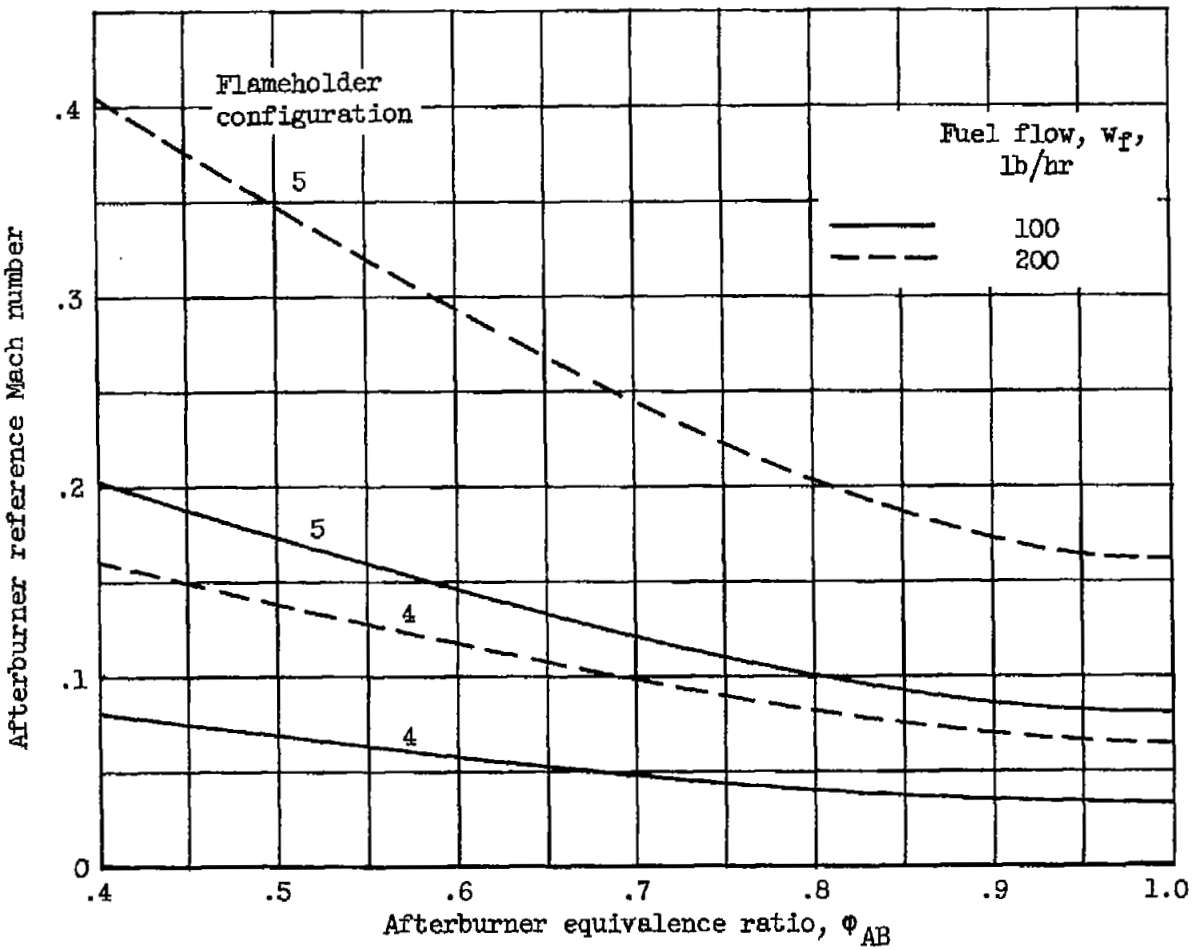

Figure 10. - Variation of afterburner reference Mach number with afterburner equivalence ratio. Inlet pressure, 30 inches of mercury absolute; inlet temperature, 80° F.

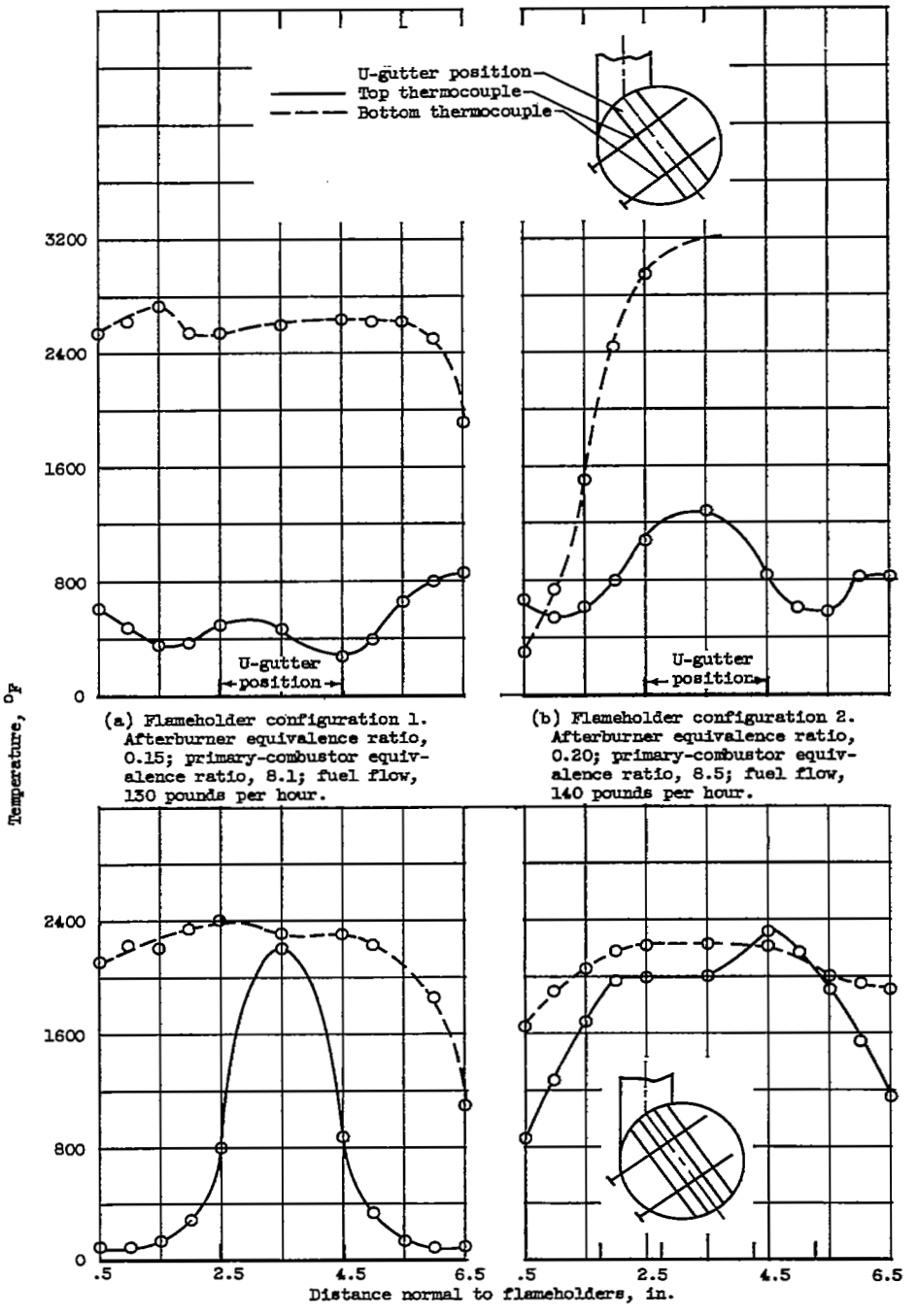

(a) Flameholder configuration 1. Afterburner equivalence ratio, 0.15; primary-combustor equivalence ratio, 8.1; fuel flow, 130 pounds per hour.

(b) Flameholder configuration 2. Afterburner equivalence ratio, 0.20; primary-combustor equivalence ratio, 8.5; fuel flow, 140 pounds per hour.

(c) Flameholder configuration 3. Afterburner equivalence ratio, 0.15; primary-combustor equivalence ratio, 8.0; fuel flow, 129 pounds per hour.

(d) Flameholder configuration 4. Afterburner equivalence ratio, 0.3; primary-combustor equivalence ratio, 20; fuel flow, 125 pounds per hour.

Figure 11. - Effect of afterburner flameholder design on afterburner outlet-temperature profile (station F-F). Inlet pressure, 30 inches of mercury absolute; inlet temperature, 80° F.

[redacted]

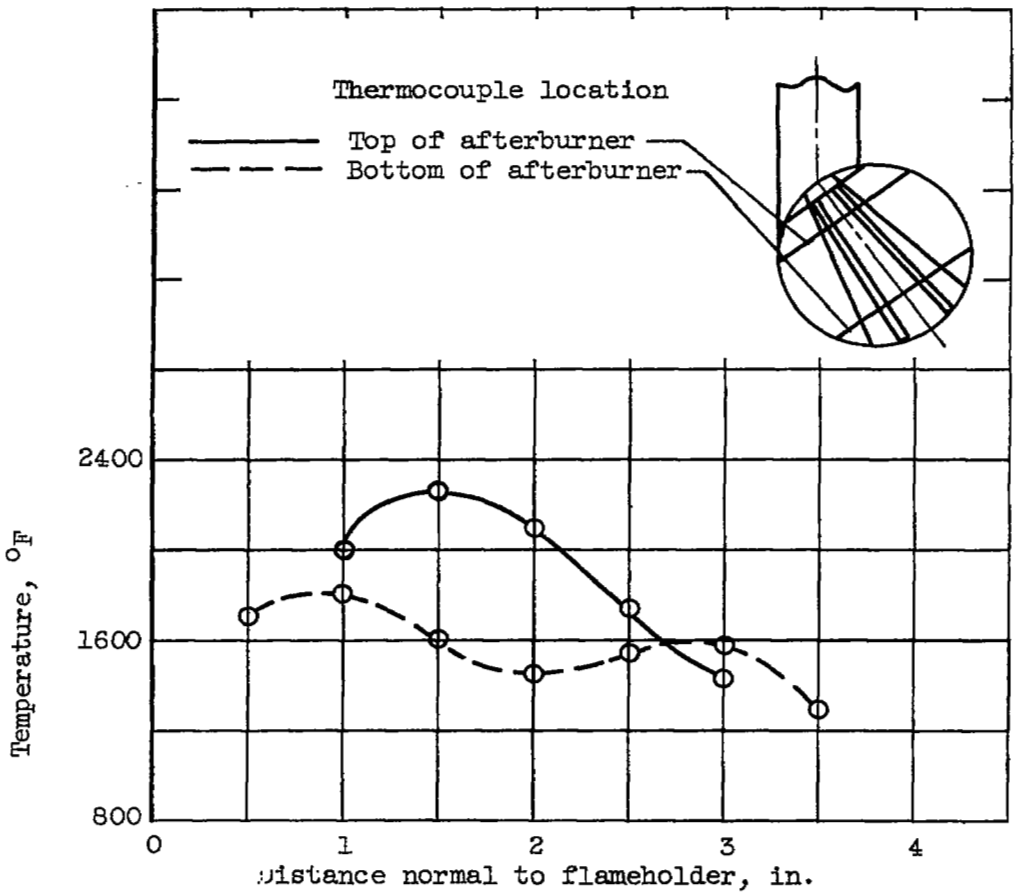

(e) Flameholder configuration 5. Afterburner equivalence ratio, 0.37; primary-combustor equivalence ratio, 16; fuel flow, 162 pounds per hour.

Figure 11. - Concluded. Effect of afterburner flameholder design on afterburner outlet-temperature profile (station F-F). Inlet pressure, 30 inches of mercury absolute; inlet temperature, 80° F.

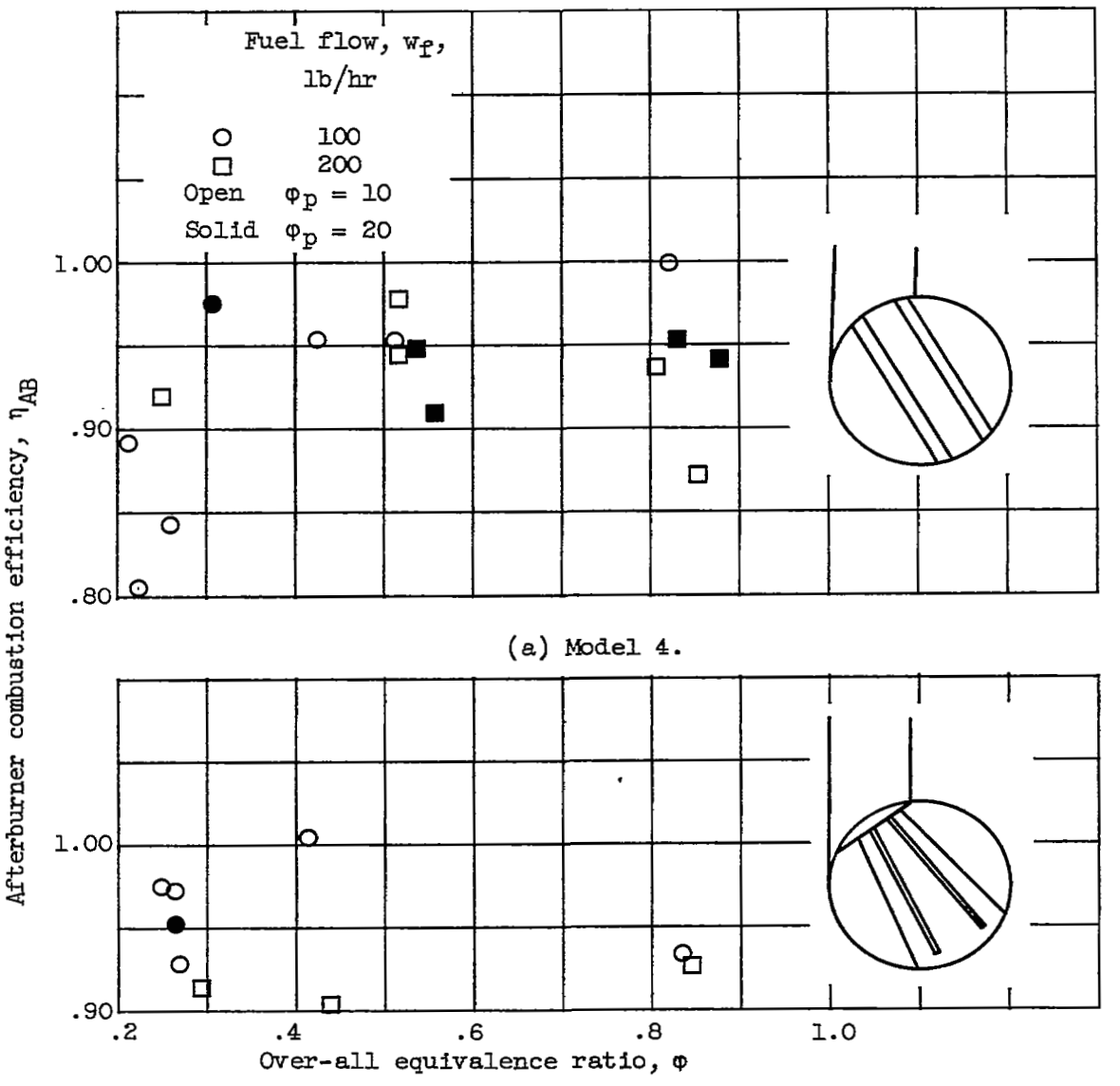

(a) Model 4.

(b) Model 5.

Figure 12. - Variation of combustion efficiency with over-all equivalence ratio for two flameholder designs. Inlet-air temperature, 80° F.

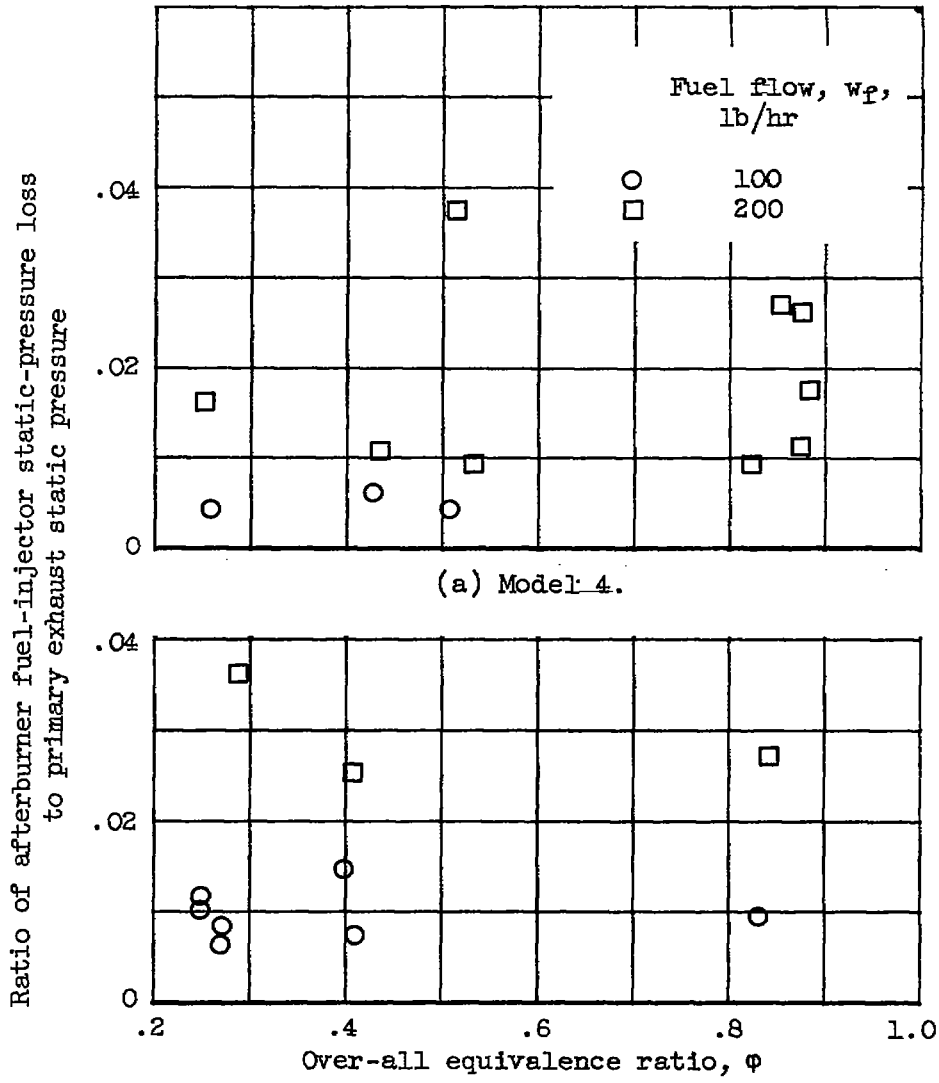

(a) Model 4.

(b) Model 5.

Figure 13. - Afterburner fuel-injector pressure loss.